Université de Montréal

Development of an Awake Behaving model for Laser Doppler Flowmetry in Mice

par **Dima Obari**

Département de pharmacologie et physiologie,
Faculté de médecine

Mémoire présenté à la Faculté des études supérieures
en vue de l'obtention du grade de Maîtrise ès Sciences (M. Sc.)
en pharmacologie

Août, 2017

Résumé

Bien que le cerveau ne constitue que 2% de la masse du corps chez les humains, il présente l'activité métabolique la plus élevée dans le corps, et en conséquence, constitue un organe hautement vascularisé. En fait, l'approvisionnement en sang dans le cerveau est strictement modulé au niveau régional par un mécanisme fondamental nommé couplage neurovasculaire (CNV), qui associe les besoins métaboliques locaux au flux sanguin cérébral [1, 2]. Notre compréhension du CNV sous des conditions physiologiques et pathologiques a été améliorée par un large éventail d'études menées chez les rongeurs. Néanmoins, ces études ont été réalisées soit sous anesthésie, soit chez la souris éveillée et immobilisée, afin d'éviter le mouvement de la tête pendant l'acquisition de l'image. Les anesthésiques, ainsi que le stress induit par la contention, peuvent altérer l'hémodynamique cérébrale, ce qui pourrait entraver les résultats obtenus. Par conséquent, il est essentiel de contrôler ces facteurs lors de recherches futures menées au sujet de la réponse neurovasculaire.

Au cours de l'étude présente, nous avons développé un nouveau dispositif pour l'imagerie optique éveillée, où la tête de la souris est immobilisée, mais son corps est libre de marcher, courir ou se reposer sur une roue inclinée. En outre, nous avons testé plusieurs protocoles d'habituation, selon lesquels la souris a été progressivement entraînée pour tolérer l'immobilisation de tête, afin de minimiser le stress ressenti lors des sessions d'imagerie. Enfin, nous avons, pour la première fois, cherché à valider l'efficacité de ces protocoles d'habituation dans la réduction du stress, en mesurant l'évolution des taux plasmatiques de corticostérone tout au long de notre étude.

Nous avons noté que les souris s'étaient rapidement adaptées à la course sur la roue et que les signes visibles de stress (luttes, vocalisations et urination) étaient nettement réduits suite à deux sessions d'habituation. Néanmoins, les taux de corticostérone n'ont pas été significativement réduits chez les souris habituées, par rapport aux souris naïves qui ont été retenues sur la roue sans entraînement préalable ($p > 0,05$).

Ce projet met en évidence la nécessité d'une mesure quantitative du stress, car une réduction des comportements observables tels que l'agitation ou la lutte peut être indicative non pas d'un niveau de stress plus faible, mais plutôt d'un désespoir comportemental. Des recherches supplémentaires sont nécessaires pour déterminer si la fixation de la tête lors de l'imagerie optique chez la souris peut être obtenue avec des niveaux de stress plus faibles, et si le stress induit par la contrainte effectuée avec notre dispositif est associé à des changements de la réponse hémodynamique.

Mots clés – débit sanguin cérébral, couplage neurovasculaire, imagerie optique, anesthésie, stress, corticostérone, souris.

Abstract

Whilst the brain only constitutes 2% of total body weight in humans, it exhibits the highest metabolic activity in the body, and as such is a highly vascularized organ. In fact, regional blood supply within the brain is strictly modulated through a fundamental process termed neurovascular coupling (NVC), which couples local metabolic needs with cerebral blood flow [1, 2]. A wide array of optical imaging studies in rodents has enhanced our understanding of NVC under physiological and pathological conditions. Nevertheless, these studies have been performed either under anesthesia, or in the awake mouse using restraint to prevent head-motion during image acquisition. Both anesthetics and restraint-induced stress have been clearly shown to alter cerebral hemodynamics, thereby potentially interfering with the obtained results [3, 4]. Hence, it is essential to control for these factors during future research which investigates the neurovascular response.

In the present study, we have developed a new apparatus for awake optical imaging, where the mouse is head-restraint whilst allowed to walk, run or rest on an inclined wheel. In addition, we have tested several habituation protocols, according to which the mouse was gradually trained to tolerate head-restraint, in order to minimize the stress experienced during imaging sessions. Lastly, we have, for the first time, sought to validate the efficiency of these habituation protocols in reducing stress, by measuring the evolution of plasma corticosterone levels throughout the study.

We noted that the mice had quickly adapted to running on the wheel, and that the overt signs of stress (struggling, vocalizations and urination) were clearly reduced within two

habituation sessions. Nevertheless, corticosterone levels were not significantly reduced in habituated mice, relative to naïve mice that were restrained on the wheel without prior training ($p > 0.05$).

This project highlights the necessity for a quantitative measure of stress, as a reduction in observable behaviors such as agitation or struggling may be indicative not of lower stress, but rather, of behavioral despair. Further research is needed to determine whether head-fixation during optical imaging in mice can be achieved with lower stress levels, and if restraint-induced stress using our apparatus is associated with changes in the hemodynamic response.

Keywords – cerebral blood flow, neurovascular coupling, optical imaging, anesthesia, stress, corticosterone, mice.

Table of Contents

List of Figures

List of Tables

Abbreviations

20-HETE	20-hydroxyeicosatetraenoic acid
2D-OIS	2-dimensional optical imaging stereoscopy
AA	arachidonic acid
ATP	adenosine triphosphate
BKCa	large conductance calcium-activated potassium channel
BP	blood pressure
BOLD	blood-oxygen-level dependent
CA	cerebral autoregulation
CBF	cerebral blood flow
CBV	cerebral blood volume
CMR	cerebral metabolic rate
CMRglc	cerebral metabolic rate of glucose utilization
$CMRO_2$	cerebral metabolic rate of oxygen utilization
COX-2	cyclo-oxygenase-2
EC	endothelial cell
EEG	electroencephalogram
EET	epoxyeicosatrienoic acid
ELISA	enzyme-linked immunosorbent assay
FMRI	functional magnetic resonance imaging
eNOS	endothelial nitric oxide synthase
IP_3	inositol 1,4,5,-triphosphate

IP3R2	inositol 1,4,5,-triphosphate receptor 2
LDF	laser Doppler flowmetry
LSCI	laser speckle contrast imaging
MAC	minimum alveolar concentration levels
MAP	mean arterial pressure
MRI	magnetic resonance imaging
NIRS	near infrared imaging spectroscopy
NMDAR	N-methyl-d-aspartate receptor
nNOS	neuronal nitric oxide synthase
NO	nitric oxide
NVC	neurovascular coupling
OFC	open field chamber
OIIS	optical imaging of intrinsic signals
PET	positron emission tomography
PGI2	prostacyclin
PGE2	prostaglandin E2
PLA2	phospholipase A2
PLD2	phospholipase D2
SPECT	single emission computed tomography
SR101	sulforhodamine-101
TPLSM	two-photon laser scanning microscopy
VSMC	vascular smooth muscle cell

Acknowledgments

I would like to extend my deepest gratitude to my supervisor **Dr. Hélène Girouard**, for her continuous support, guidance and kindness, which have forever shaped my personal and professional development. Thank you for always being there and believing in me, for all the opportunities and enriching experiences that you've granted me, and for the invaluable knowledge that I've been able to acquire in your lab. It's been a true honor to be your student. I have grown so much during these past two years, and I can only hope to make a similar impact on another person's life, someday along the line.

I'd like to also express sincere thanks to **Dr. René Cardinal** for his continued support, and the members of my thesis committee, **Dr. Éric Thorin** and **Dr. Christopher Rose**, for sharing their critical insights. I also thank **Dr. Lesage's laboratory** for an enriching collaboration, and for their contribution with the head-restraint device and the open field chamber.

This dissertation would also have not been possible without the help and support of **Diane Vallerand**, who was present through every step of this process, and was always extremely kind, supportive, and definitely a real pleasure to work with!

Thanks to my dear friends and colleagues – **Sherri**, **Gervais** and **Xuewei** – with whom I've shared countless laughs and precious moments, right from the start. You guys are the best.

Thanks to all members of the Cerebrovascular lab – **Lin, Sonia, Stéfane, Nasr, Maryam, Florencia** and **Adrián** – you're my second family, and I am grateful to have shared this part of my life with you.

Very special thanks to my **family** for their support and for always believing in me, and to **all of my friends** for being there every step of the way.

Last, but certainly not least, I'd like to thank my fiancé, **Anas Wattar**. Thank you very much for your continued love and support throughout this process… I can't wait to walk down that isle with you.

Introduction

Overview

We first provide a general description of the major arteries that supply blood to the brain, and how they divide into progressively smaller vessels which penetrate deep into the parenchyma (**Section 1**). As we will see, blood flow through cerebral vessels is strictly modulated by a dynamic and complex interplay between different regulatory mechanisms including cerebral autoregulation and neurovascular coupling, which act to ensure constant supply of energy to neural tissue (**Section 2**).

Whilst much of the research on the regulation of cerebral blood flow (CBF) has been achieved *in vivo* using anesthetized animals, anesthetics have been demonstrated to exert significant effects on the CBF. We discuss how different types of anesthetics alter cerebral hemodynamics and metabolism, as well as neural dynamics, brain physiology and bodily homeostasis (**Section 3**). We then introduce several imaging modalities which are commonly used to investigate neurovascular coupling, and have been used in awake behaving studies in order to avoid the effects of anesthesia on CBF (**Section 4**).

Because imaging in the awake, restrained animal is often associated with increased stress levels, it is important to understand the effects of stress on CBF. In our last section, we discuss the effects of different types of anesthetics on cerebral hemodynamics, resting brain metabolism, neuronal and glial dynamics, cerebral physiology and bodily homeostasis, and how these effects in turn can modulate the neurovascular response to sensory stimulation in rodents (**Section 5**).

1. Anatomy and Ultrastructure of the Cerebral Vasculature

1.1 Major Arteries of the Brain

While the brain only constitutes 2% of the human's bodyweight, it exhibits remarkable metabolic activity, consuming a colossal one fifth of the body's total energetic expenditure. As such, it is no surprise that the brain is a highly vascularized organ. In fact, with every passing minute, the heart supplies the central nervous system (CNS) with 0.75 liters of warm blood, gushing from the left ventricle into the aortic arch and through two sets of large arterial branches: the left and right common carotid arteries, and the left and right subclavian arteries (**Figure 1**), which serve the anterior and posterior aspects of the brain, respectively [5].

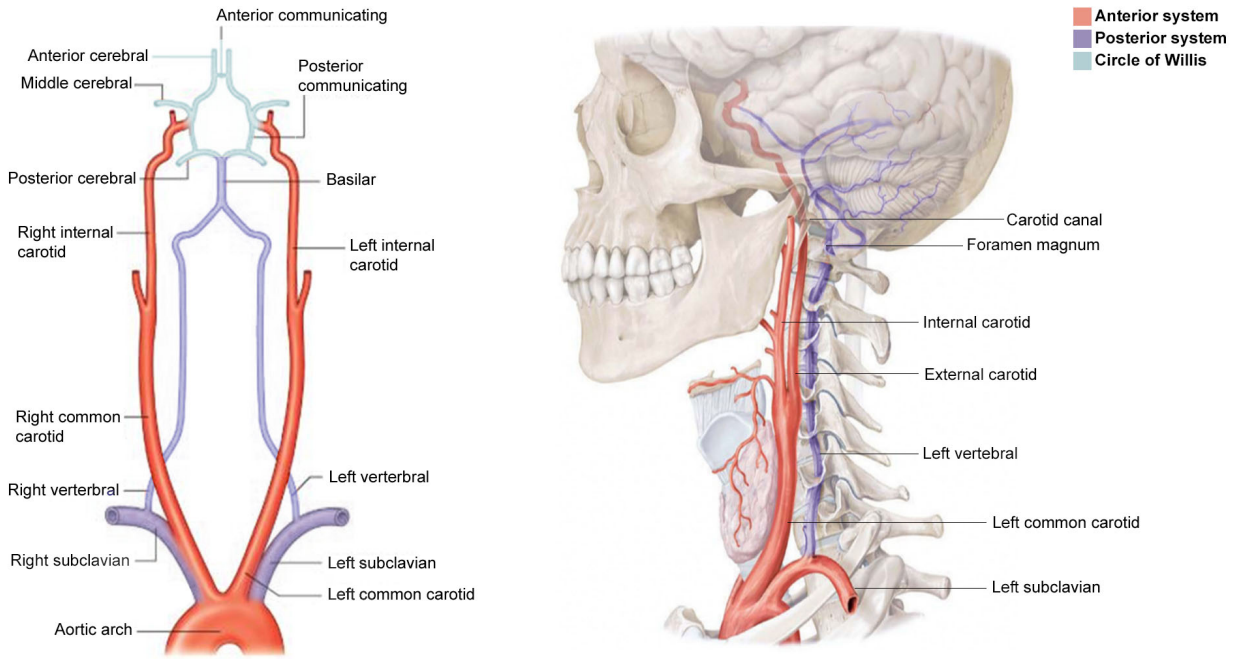

Figure 1. Arterial blood supply: from the aortic arch to the brain.

The brain is perfused by two sets of large arteries: the internal carotids (anterior system) and the vertebral arteries (posterior system). The latter merge into the basilar artery and join at the base of the brain with the internal carotids and communicating arteries, forming the circle of Willis (figure adapted from [6] and [7]).

Anteriorly, the common carotid arteries give rise to bilateral external and internal carotids. The **internal carotid arteries** supply the anterior part of the cerebrum, providing the vast majority of the cerebral blood flow (CBF) (80%). These run upward the neck and enter the skull through the carotid canal. They then pierce into the dura mater and enter the subarachnoid space, where they bifurcate into their terminal branches, the anterior cerebral arteries and middle cerebral arteries. Posterior to the carotid arteries, the subclavian system branches out into the left and right **vertebral arteries**, which supply 20% of the CBF. These arteries penetrate the cranium through the foramen magnum, and merge medially into the single basilar artery, which terminates by splitting into the bilateral posterior cerebral arteries (**Figure 1**).

The anterior, middle and posterior cerebral arteries fuse together through anterior and posterior communicating arteries into an anastomotic ring located at the base of the brain, known as the **Circle of Willis** (**Figure 1**). This arterial ring allows for blood reaching one hemisphere to circulate around the ring and perfuse the opposite side of the brain [8], thus enabling continued cerebral perfusion in the event of occlusion or stenosis of the internal carotid or vertebral arteries [9].

1.2 Intracerebral Vessels

1.2.1 Architecture of the Cerebrovascular Tree

As they leave the circle of Willis, the large intracranial arteries run along the surface of the brain, and branch out into pial arteries and progressively smaller arterioles and capillaries (**Figure 2**).

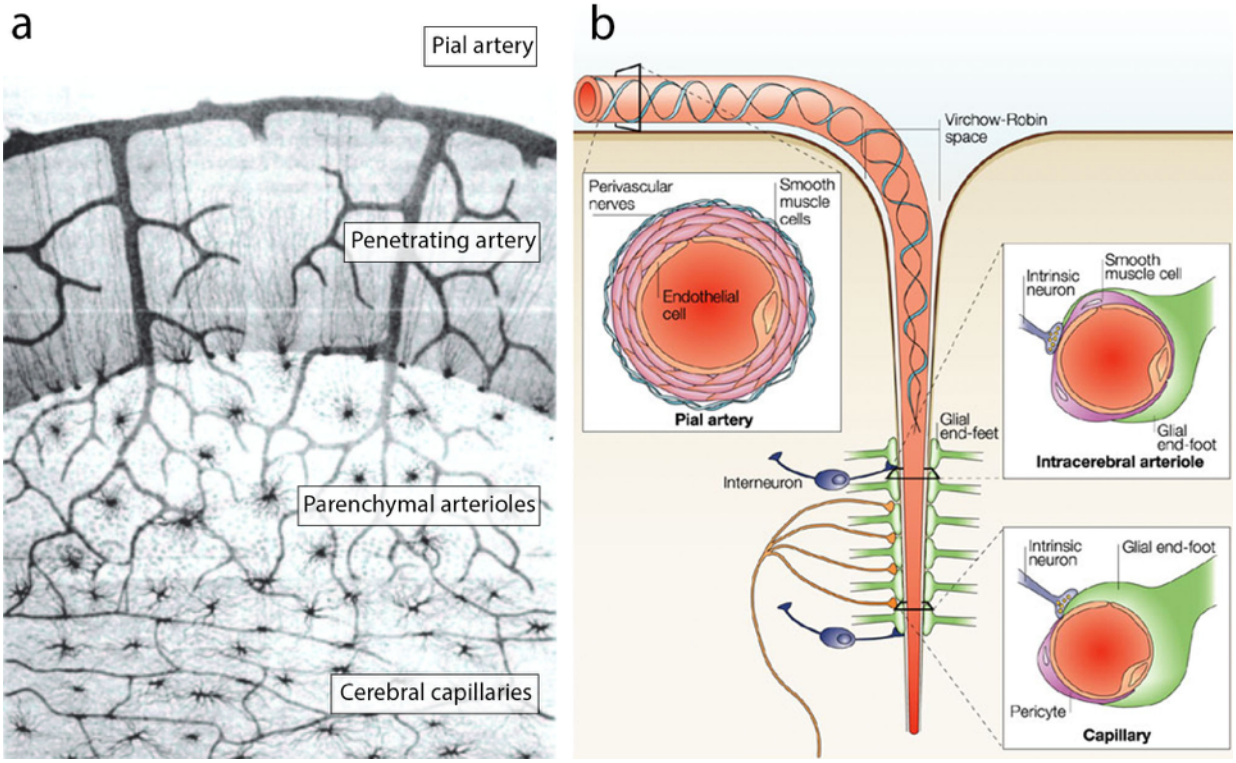

Figure 2. Moving down the cerebral vasculature.

a) Illustration by Camillio Golgi (1843-1926) detailing branches of the vascular tree, from the cortical surface down to the microvascular bed. b) Pial arteries penetrate into the Virchow-Robin space and come in direct contact with the astrocytic endfeet as they dive deeper into the brain tissue (figure adapted from [10] and [1]).

Pial arteries are large vessels (200-1000 µm diameter in humans) which lie atop of the pia mater (innermost layer of the cerebral meninges), and consist of an innermost layer of endothelial cells (ECs), vascular smooth muscle cells (VSMCs) [5], and an outer layer termed adventitia [11]. These arteries dive into tissue at a right angle to the brain surface and give rise to **penetrating arteries** (40-200µm), which reach an extension of the subarachnoid space termed Virchow-Robin. As the penetrating arteries reach further into the tissue, this space disappears, and the parenchymal arterioles become closely associated with astrocytic endfeet. At the bottom of the cerebrovascular tree, **capillaries** (7-9 µm) form a dense network consisting of a continuous layer of ECs, surrounded by pericytes and a basal membrane on which astrocytic processes are apposed [11].

1.2.3 Perivascular Innervation

Throughout the cerebral vasculature, nerve fibers are intimately associated with the vessel wall components (**Figure 3**). Pial arteries at the surface of the brain are supplied by **extrinsic nerve fibers** from the autonomous nervous system [12, 13]. As they dive into the brain tissue, penetrating arteries lose their peripheral nerve supply and, once they move past the Virchow-Robin space, receive **intrinsic innervation** from within the neuropil. These neurons may signal through the astrocytes which surround the parenchymal vessels, causing the latter to vasodilate in response to neuronal activity. This association between neuronal needs and CBF is termed neurovascular coupling (NVC) [14] and will be addressed in **Section 2.3**.

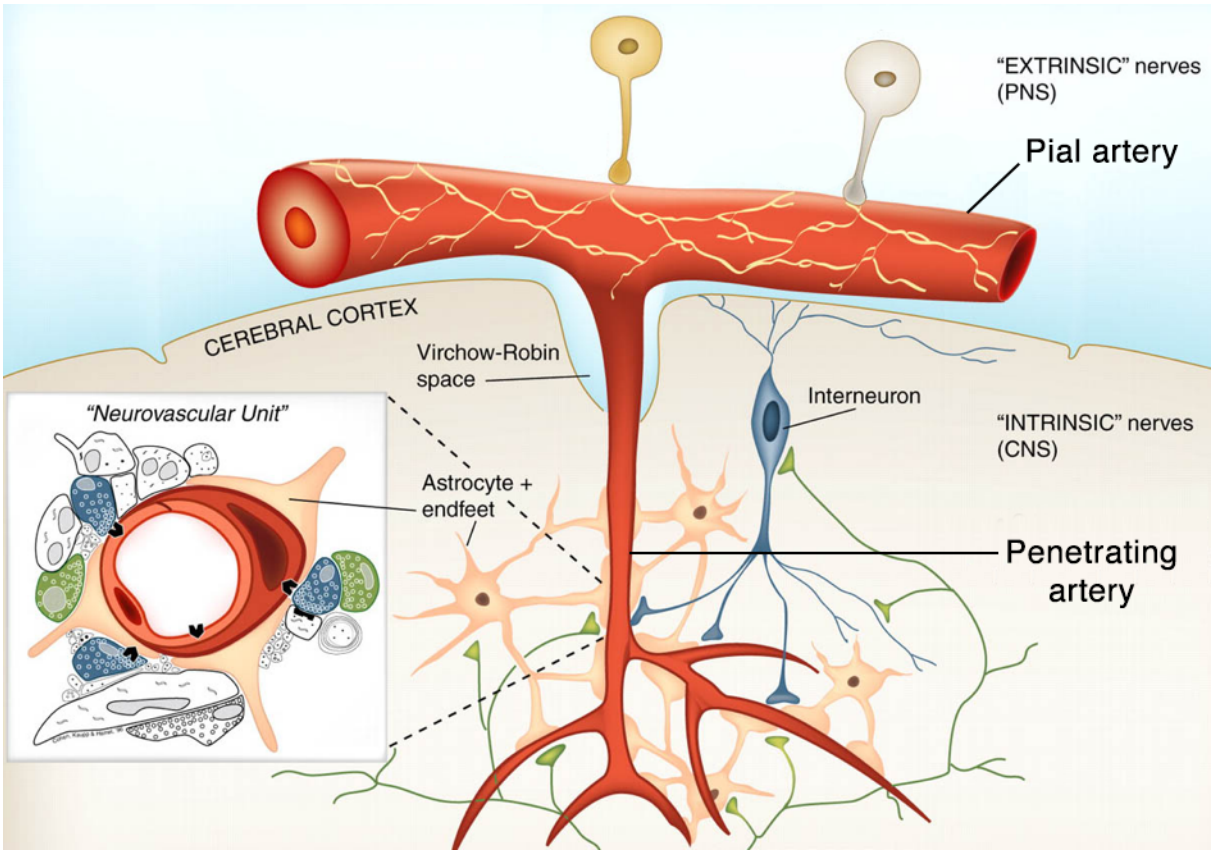

Figure 3. Perivascular innervation of cerebral blood vessels.

Pial arteries receive extrinsic innervation, whereas parenchymal arteries receive afferents from local cortical interneurons or subcortical neurons (figure adapted from [13]).

2. Regulation of Cerebral Blood Flow

Whilst the brain is one of the body's most metabolically active organs (see **Section 1.1**), neurons store little energy as glycogen and relies almost entirely on circulating glucose as a source of fuel. As a result, even minor decreases in blood supply can disrupt brain function and yield irreversible damage to the cellular structures within minutes [15]. Conversely, pathological increases in CBF can cause cerebral edema, which would increase intracranial pressure and lead to severe neurologic complications and death [15]. It follows that strict control of CBF is absolutely critical, in order to ensure a constant and adequate supply of glucose and oxygen to the neural tissue, whilst preserving normal ranges of cerebral blood volume (CBV) and intracranial pressure. Hence, the brain is endowed with two regulatory mechanisms of CBF – cerebral autoregulation (CA) and neurovascular coupling (NVC) – which will be discussed below.

2.1 Cerebral Autoregulation

CA is the process by which CBF is maintained constant despite fluctuations in perfusion pressure [16]. In normotensive adults, cerebral perfusion is maintained at ~50 mL per 100g of brain tissue per minute, when mean arterial pressure (MAP) is within the range of **50 – 150 mmHg** [17]. Above and below this range, the protective autoregulatory response is lost and the relationship between CBF and MAP becomes linear [18, 19] (**Figure 4**).

CA is proposed to be mediated by myogenic and neurogenic mechanisms. The **myogenic response** refers to the intrinsic ability of VSMCs to counteract normal fluctuations in blood pressure (BP) which occur during everyday activities such as sleep, changes in posture and exercise [20]. This is achieved through the constriction and dilation of large cerebral arteries and arterioles in response to increases and decreases in intraluminal pressure, respectively [18, 21]

(**Figure 4**). Since the myogenic response is maintained in vessels denuded of endothelium [22] and in sympathetically and parasympathetically denervated animals (cats) [23], this mechanism is considered inherent to VSMCs and independent of neural and hormonal factors [24].

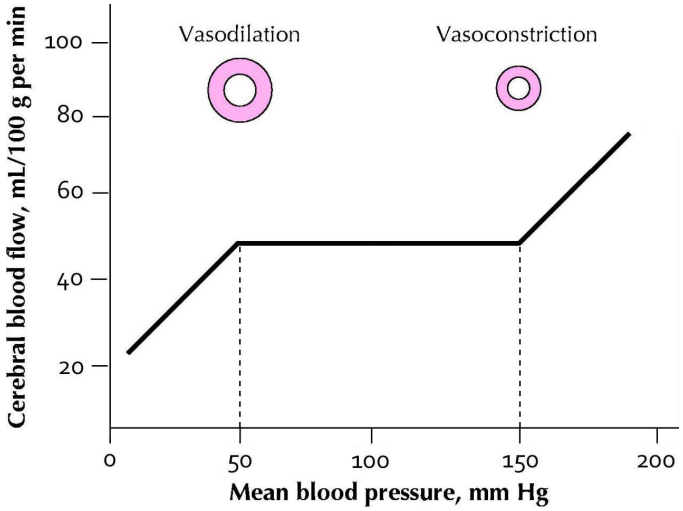

Figure 4. Autoregulation of blood flow with changing blood pressure.

Cerebral perfusion is maintained at a constant value of 50 mL per 100g of brain tissue per minute via CA, provided mean arterial pressure is within the autoregulatory range of 50 – 150 mmHg. Above and below the autoregulatory range, CA is lost and CBF passively follows the perfusion pressure (figure adapted from [25]).

Neurogenic control is thought to intervene during challenging during challenging circumstances, when the myogenic mechanism of CA has been overwhelmed. Indeed, the large extracranial arteries and pial arteries are extensively innervated by both the sympathetic and parasympathetic branches of the autonomous nervous system [26] (see **Section 1.2.3**), which have been shown to alter the limits of the autoregulatory response [23, 27]. It has been proposed that during acute hypertensive states, the sympathetic branch is activated and increases vascular tone [28], thereby protecting the microvasculature against damage and rupture. However, if the arterial pressure exceeds 200 mmHg, the cerebral vessels are no longer able to constrict, and the CBF follows changes in perfusion pressure passively [29].

2.2 Neurovascular coupling

Whilst the aforementioned mechanisms of CA are aimed at keeping the CBF within a predetermined autoregulatory range, NVC provides a dynamic modulation of local blood flow, whereby neuronal activity induces a regional increase in CBF in order to match local energetic demands [30, 31]. This mechanism is mediated through various metabolic pathways which involve neurons, astrocytes and pericytes.

2.2.1 Neuronal Signaling

Neurons are proposed to constitute the driving force behind NVC, due to their elevated energy consumption during neurotransmission [32], in addition to the important role of glutamatergic transmission [33, 34] and receptor activation [35, 36] in eliciting a rapid increase in CBF.

In fact, the release of **glutamate** during neuronal activity has been found to activate N-methyl-d-aspartate receptors (NMDARs), leading to Ca^{2+} influx into neurons and the synthesis of nitric oxide (**NO**) by neuronal nitric oxide synthase (nNOS), which elicits dilation of the VSMCs [37, 38] (**Figure 5**). Indeed, NO induces vasodilation both in brain slices and *in vivo*, and inhibition of NO synthesis in the cortex has been shown to attenuate the CBF increases that follow neuronal activity [39], thus confirming its role in NVC.

2.2.2 Astrocytic Signaling

It is no surprise that astrocytes are also implicated in NVC, as they are ideally positioned to transduce neuronal signals into a vascular response. Indeed, astrocytic endfeet cover about 99% of the abluminal surface of blood vessels [40], and a single astrocyte can contact up to 140,000 synapses [41].

Accordingly, ATP released during neuronal activity was shown to stimulate astrocytic **P2X1** receptors, leading to an increase in astrocytic Ca^{2+} and the activation of phospholipase D2 (**PLD2**). This results in the synthesis of vasoactive arachidonic acid (**AA**) derivatives and subsequent vasodilation (**Figure 5**).

In addition to activating PLD2, elevations in astrocytic Ca^{2+} can also induce vasodilation through the opening of **BKCa** channels [42], which results in K^+ efflux into perivascular space [43, 44]. The subsequent increase in extracellular K^+ activates inwardly rectifying K^+ channels and induces vasodilation [45-51] (**Figure 5**).

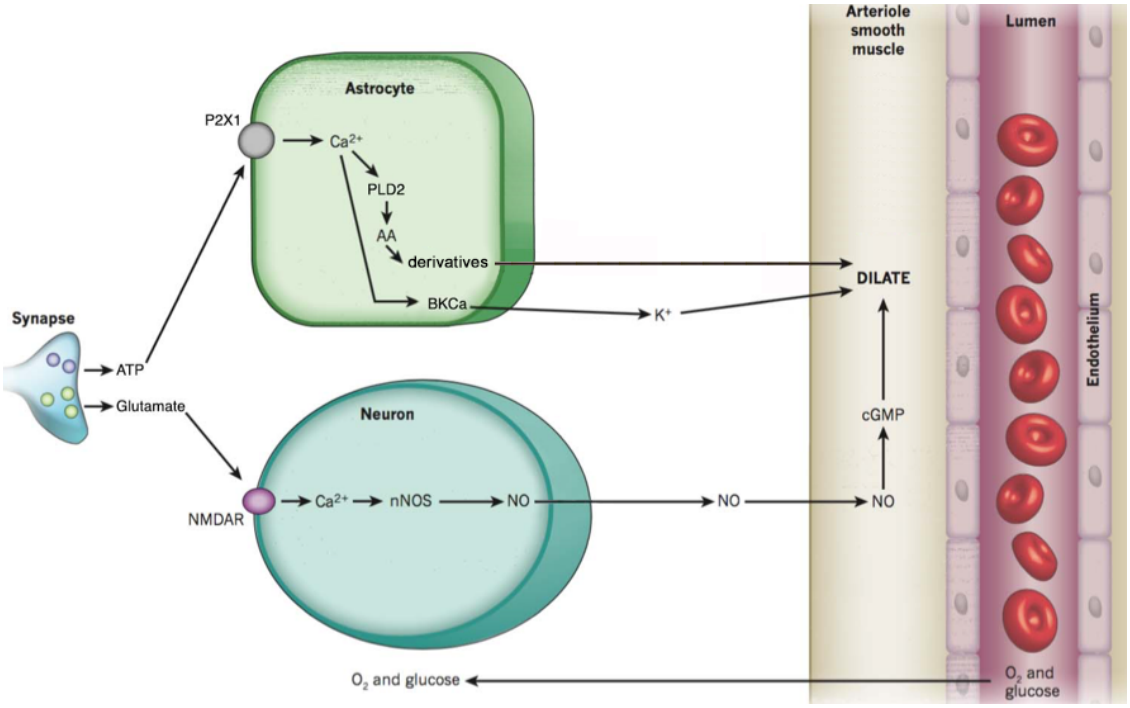

Figure 5. Major pathways of neuron and astrocyte-mediated neurovascular coupling.

Neural activity may induce an increase in CBF through the release of (1) glutamate, which acts on neuronal NMDAR to elicit synthesis of vasodilatory NO, and (2) ATP, which activates astrocytic P2X1 receptors to induce production of vasoactive AA derivatives, and the release of K^+ which has strong dilatory effects on the vasculature. These interactions between neurons, astrocytes and vascular cells effect changes in cerebral blood flow, in a bid to match the delivery of glucose and oxygen with the local energetic needs. AA, arachidonic acid; BKCa, large conductance Ca^{2+}-activated K^+ channel; cGMP, cyclic guanosine monophosphate; NMDAR, N-methyl-D-aspartate receptor; nNOS, neuronal nitric oxide synthase; NO, nitric oxide; PLD2, phospholipase D2; (figure adapted from [52]).

2.2.3 Role of Pericytes

Pericytes, a type of vascular mural cells which wrap around cerebral capillaries [53], possess contractile properties similar to VSMCs [54], and thus may contribute to NVC by modulating capillary diameter. Indeed, several *in vitro* experiments have subsequently shown pericytes to respond to vasoactive substances such as AA derivatives, and to induce localized vasoconstrictions [55]. Since on average, neurons are anatomically closer to capillaries (8-23 μm) than to arterioles (70–160 μm), these properties of capillary vessels would allow the vascular network to respond to changes in metabolic demands at a more local level [56]. Subsequently, pericytes could propagate the vascular response to upstream arterioles through gap junctions between the pericytes themselves or between pericytes and the underlying endothelium [55].

It is possible that the signaling pathways which govern the dilation and constriction of pericytes are similar to those established for VSMCs, and implicate Ca^{2+}-dependent synthesis and release of vasoactive AA derivatives from astrocytes (**Figure 10**). However, these dynamics remain to be explored.

3. Effect of Anesthetics on Cerebral Blood Flow

Thus far, most studies on CBF regulation and NVC have been conducted *in vivo* under anesthesia. Indeed, anesthetics have been widely used during image acquisition, in order to minimize motion artifacts and prevent the induction of stress in the animals (see **Section 5**). Further, anesthetic preparations have the advantage of enabling the rigorous monitoring of physiological parameters, such as blood gases (pO_2 and pCO_2), pH and pressure. This is usually achieved in acute studies with rodents through invasive procedures such as the cannulation of the femoral artery, which allows to continuously monitor the BP through an attached pressure transducer, and artificial ventilation, which is an effective method for maintaining blood gas levels within the physiological range [57].

In spite of the significant role anesthetics have played in neurovascular research, studies increasingly show that anesthesia produces a neurological condition that is distinct from any physiological state, leading to broad physiological changes and importantly, significant alterations in the hemodynamics response. This is particularly apparent in mice, which display poor reproducibility and inconsistent NVC in comparison with rats and other species [58-64]. In this section, we discuss the effects of different types of anesthetics on cerebrovascular dynamics, resting brain metabolism, neuronal and glial dynamics, and how these effects in turn can modulate the neurovascular response to sensory stimulation in rodents.

3.1 Cerebral Hemodynamics

Studies have found anesthesia to affect the neural-vascular relationship in rodents in a number of ways. First, the **amplitude** of the hemodynamic response was found to be approximately four times smaller in rodents anesthetized with urethane (1 – 1.25 g/kg) compared with

unanesthetized rodents, both subsequent to visual [62] and sensory stimulation [65]. Similar findings were obtained with α-chloralose (60 mg/kg) and propofol (0.8 mg/kg/min), whereby the size of the activation area in the brain and the BOLD response were significantly reduced following limb stimulation [66, 67].

Second, the **spatial dynamics** of the neural-vascular response have been shown to differ markedly between different anesthetic conditions. For instance, cortical mapping with intrinsic imaging created focal localization under pentothal, whereas anesthesia with isoflurane produced broader and more heterogeneous activation maps in the monkey somatosensory cortex [68].

Last, anesthetics also interfere with the **temporal dynamics** of the response, with responses in anesthetized animals increasing more slowly, peaking later, and taking more time to return to baseline compared with awake animals [69]. Indeed, the BOLD responses subsequent to hindpaw stimulation in mice had markedly different shapes under distinct anesthetic regimes (isoflurane, medetomidine, propofol and urethane) [70].

Hence, anesthesia exerts considerable influence on cerebral hemodynamics, affecting the size, spatial coordination and temporal profile of the hemodynamic response, with different effects depending on the type and dosage of anesthetic used.

3.2 Brain Resting Metabolism

It is well known that the brain exhibits a particularly high metabolic demand (see **Section 2**). However, nearly all anesthetics have been shown to drastically reduce the basal **cerebral metabolic rate** (CMR) in a dose-dependent manner. CMR is usually assessed in terms of variations in **glucose utilization** (CMRglc), measured using 2-deoxyglucose in animals [71].

In particular, general anesthetics such as isoflurane and halothane have been demonstrated to decrease CMRglc through inhibitory actions on mitochondrial ATP synthesis in rats [72] and mice [73]. Effectively, isoflurane was shown to reduce CMRglc in rats by 11%, 70%, 74% and 81% compared with the awake state, at the respective isoflurane minimal alveolar concentration (MAC) levels 0.5, 1.0, 1.5 and 2.0 [74, 75]. Further, α-chloralose (60 mg/kg) [76-78], pentobarbital (10 or 30 mg/kg) [79, 80] and phenobarbital (150 mg/kg) [81] were found to attenuate CMRglc by ~40-55% relative to the awake condition, especially in regions which exhibit high metabolic activity such as the cortex.

Anesthesia-induced changes in CMR have been shown to affect normal **cerebral oxygenation**. Indeed, researchers have found substantial variability in the tissue oxygenation under anesthesia [82], which hinders comparisons between the awake and anesthetized conditions. Furthermore, using a recently developed two-photon phosphorescent probe which provides micron-scale measurements of cerebral oxygenation, Lyons and colleagues showed oxygen tension to be greatly enhanced under 2% isoflurane [83]. Effectively, since most general anesthetics suppress CMR in a dose-dependent manner, it is expected that anesthetics will decrease the cerebral utilization rate of oxygen, thus leading to a rise in the oxygenation of brain tissue [84].

3.3 Neuronal, Glial and Vascular cells

Since most anesthetics drastically attenuate cerebral metabolism, it is only to be expected that they would also dampen neuronal activity. In fact, anesthesia has been shown to exert strong inhibitory effects over baseline firing in **neurons** [85-88]. Specifically, anesthesia causes neurons to hyperpolarize by increasing inhibition and decreasing excitation [89, 90]. Indeed, whilst

synaptic inhibition in awake animals is similar to excitation in amplitude, in the anesthetized state, inhibition was shown to be much stronger than excitation [91-93]. The increase in synaptic inhibition observed under anesthesia is thought to be mediated through common pathways which involve the potentiation of GABA and glycine-mediated inhibitory transmission, and the suppression of glutamatergic excitatory transmission [94].

As a result, anesthetized animals exhibit oscillations (1 Hz) between a depolarized up-state, which resembles the sustained depolarization in awake animals, and a hyperpolarized down-state, during which synaptic activity is completely suppressed for a brief duration (~0.1 second). These changes in neuronal firing patterns are reflected in EEG recordings by a shift from high-frequency, low-amplitude EEG activity, to low-frequency, high amplitude patterns resembling NREM sleep [95, 96]. Accordingly, mice anesthetized with isoflurane (1.0-1.5%), ketamine-xylazine (120 mg/kg and 10 mg/kg) or urethane (1250 mg/kg) exhibited significantly altered electrocorticographic activity, with slower-frequency spiking compared with awake mice [97]. Similarly, anesthetizing rats with halothane (0.7-1.5%) lead to a dose-dependent increase in delta waves, indicative of a depressed basal neuronal activity [87, 88]. Nevertheless, the effect of anesthetics on neuronal activity is not uniform across the brain. Rather, anesthesia was shown to influence spontaneous cortical activity in a region- and depth-dependent manner. Indeed, both isoflurane (1.5%) and ketamine (30 mg/kg and 1-2 mg/kg) exert a greater and more uniform modulation of frontal areas, in comparison with a preferential modulation of layer IV of the cortex in sensory brain regions [96, 98, 99].

In addition to dampening neuronal activity, anesthetics also greatly reduce the Ca^{2+} signaling frequency in **astrocytes** [97, 100]. This is a critical issue, since astrocytes play an

essential role in supporting neuronal function (e.g. by supplying them with nutrients) and mediating the neurovascular response to sensory stimulation (see **Section 2.2.2**). Indeed, anesthetizing mice with isoflurane (1.0-1.5%), ketamine-xylazine (120 mg/kg and 10 mg/kg) or urethane (1250 mg/kg) reduces Ca^{2+}-transient frequency by a factor of 10, bringing it down from 2.33 in the awake state to 0.24-0.39 mmHz per cell under anesthesia. Nevertheless, how anesthesia alters the role of astrocytes in NVC needs to be further explored.

Last, some anesthetics have been shown to exert direct effects on **vascular cells** in the brain. Indeed, most volatile anesthetics (isoflurane, desflurane and halothane) are known to have potent vasodilatory properties, in spite of their depressive effect on cerebral metabolism. Accordingly, anesthesia with isoflurane (0.5 – 1.5 MAC) was found to induce a dose-dependent relaxation of canine cerebral arteries [101, 102] through the activation of ATP-sensitive K^+ channels [103] and a decrease in Ca^{2+} signals by blocking Ca^{2+} channels in VSMCs [104-106]. Similarly, halothane is thought to promote vasodilation by depleting sarcoplasmic Ca^{2+} stores in VSMCs [107, 108] and triggering the release of relaxing factors from ECs [109]. Hence, a known disadvantage of using volatile anesthetics is that they increase CBF whilst decreasing cerebral metabolism, leading to altered dynamics between neuronal activity and vascular responses [110].

To conclude, anesthetics have been widely used to investigate the hemodynamic in animal models *in vivo*, leading to significant improvements in our understanding of the pathways which underlie NVC in physiological and pathological conditions [52]. That said, anesthetics exert considerable influence on cerebral metabolism, neuronal and glial dynamics, thereby altering neural-vascular dynamics and affecting the reproducibility of the hemodynamic

response (see **Section 3.1**). Hence, caution is required when comparing data from different studies or generalizing experimental results from the anesthetized animal to the awake human. Fortunately, recent technical advancements have facilitated the use of optical imaging modalities in the awake, unrestrained animal, thus enabling researchers to investigate critical aspects of CBF regulation and NVC under more appropriate conditions.

4. Optical Imaging Techniques for Evaluating the Hemodynamic Response in Awake Behaving Rodents

As previously discussed, the regulation of CBF involves a dynamic and complex interplay between different mechanisms, which act to ensure constant perfusion of the brain parenchyma and an adequate supply of oxygen and nutrients to active neurons. Investigation of these mechanisms has been made possible owing to optical imaging techniques, which provide powerful tools for monitoring regional hyperemic changes in both small animals and humans [111-113]. Specifically, Laser Doppler flowmetry (LDF) is the most commonly used optical imaging technique for monitoring CBF, and hence will be described in depth in the sections below. We also provide a brief review of several other optical techniques that are commonly used for intraoperative imaging of CBF and the neurovascular response in awake behaving rodents, including laser speckle contrast imaging (LSCI), optical imaging of intrinsic signals (OIIS), two-dimensional optical imaging spectroscopy (2DOIS) and two-photon laser scanning microscopy (TPLSM) (see **Table 1** for a comparison between these modalities). Last, we discuss how these technologies can be combined with other imaging modalities and optogenetic techniques to yield complex information on the cerebrovascular response.

Table 1. Comparison between different optical imaging techniques commonly used for evaluating NVC in rodents.

Technique & Principle	Spatial Resolution	Temporal Resolution	Penetration Depth	Advantages	Limitations
Laser Doppler Flowmetry (LDF) Light scattered by moving erythrocytes undergoes a *Doppler shift* proportional to their velocity [114].	Since LDF is a single-point measurement technique, it provides **no spatial information**.	**< 100 ms**	Up to **2 mm** with infrared light. Additionally, the probe can be positioned deep in the brain to image the desired structure (e.g. hippocampus)	. Easy to use . High temporal resolution . May be performed in deep brain structures . Availability of awake models	. No spatial information . No absolute measurement . Motion sensitive
Laser Speckle Contrast Imaging (LSCI) Light scattered by moving erythrocytes produces a time-varying *speckle* pattern, which is converted to 2D blood flow maps [114, 115].	Wide field of view with a spatial resolution of **~5 µm**	**10 – 50 ms**	**0.5 – 1.0 mm**	. High spatiotemporal resolution . Visualization of vascular morphology . Very practical & economic . Miniaturized version available	. No absolute measurement
Optical Imaging of Intrinsic Signals (OIIS) Neural activity induces a cascade of events which increase the tissue's absorption of light, leading to a darkening of the cortex [116].	Images large areas of the cortex (**~25 mm²**) with a spatial resolution up to **50 µm**.	**~100 ms**	Up to **2 mm** with infrared light	. High spatiotemporal resolution . Images large areas of the cortex (~25 mm^2) . Can map different physiological parameters (neural activity, HbO, HbR and CBV) depending on wavelength used. . Miniaturized version available	. Motion sensitive . Vascular artifacts
Two-Photon Scanning Laser Microscopy (TPLSM) The blood plasma is labeled with a fluorescent dye, which is excluded by RBCs and excited through the absorption of two laser photons [57, 117].	< **1 µm** (0.1 µm with super-resolution techniques [118])	A few **microseconds**	Up to **1 mm** with infrared light, or in the **cm** range with gradient index lenses	. Images at the single capillary & subcellular level . Simultaneous imaging of neuronal & glial activity, vessel diameter and RBC velocity . High level of precision . Miniaturized version available	. Images small regions . Photo-bleaching & cell damage

4.1 Laser Doppler Flowmetry (LDF)

Laser Doppler flowmetry (LDF) is an optical imaging technique which provides continuous, real-time evaluation of blood flow in cerebral vessels [119-122]. This technique is based on the **Doppler shift**, which describes the change in the frequency of a wave, subsequent to relative movement between the source of the wave and the observer. This technique is routinely used in clinical [123-126] and experimental applications [127-133] involving CBF measurement.

4.1.1 Theoretical Background

A common example of Doppler shift phenomenon is the variation in the pitch of a siren noise from an emergency vehicle as it passes by; the received frequency of the sound waves is highest during the vehicle's approach, and lowest whilst the vehicle is moving away. This is because as the vehicle is approaching, each successive sound wave is emitted in greater proximity to the observer than the previous wave. Thus, the time needed for the successive waves to reach the observer is progressively reduced, causing the sound waves to combine and resulting in a greater sound frequency. Conversely, when the vehicle is receding, the successive waves take longer to reach the observer, which causes the waves to spread out and leads to a reduced frequency.

Because this change in frequency is contingent on the relative velocity of the source of the wave and the observer, the Doppler shift can be used to measure velocities. This relationship between the original frequency (f), the shifted frequency (f'), the relative velocity of the source and the observer (v) and the wave's velocity (c) can be summarized in the equation below [114]:

$$f' - f = \frac{v}{c} f$$

This mechanism of wave propagation also applies to light; in fact, the optical Doppler shift constitutes the underlying principle of several imaging methods including ultrasound Doppler [134] and LDF [135]. In the latter technique, a small fiber-optic laser probe (diameter 0.5 – 1 mm) is placed over the cerebral cortex at the desired position for CBF measurement. This probe emits a beam of monochromatic laser light with a wavelength ranging between 670 and 810 nm, which is above the absorbance spectrum of erythrocytes and below that of water. This light is transmitted to the target tissue, and is absorbed and reflected by static and dynamic cells. Specifically, when the emitted light is absorbed by erythrocytes coursing through the cerebral blood vessels, the light's wavelength due to the movement of these cells, resulting in a Doppler frequency shift (**Figure 6**) [114, 136, 137]. The magnitude of this shift is commensurate with the number and velocity of the moving cells. Hence, when the backscattered photons are received by the photodetector, the obtained signal is processed and the blood flow velocity can be deduced following Bonner and Nossal's algorithm [137]. Due to the diffuse scattering of light within tissue, the LDF signal is independent of the flow's direction. In fact, LDF is used to evaluate relative variations in CBF with the presumption that flow geometry does not change [131].

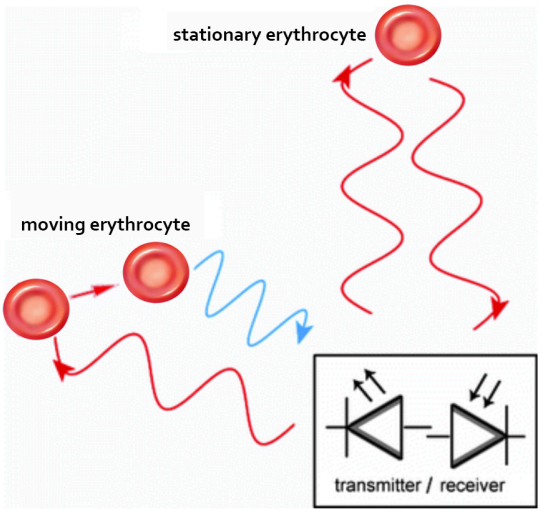

Figure 6. Principle of Laser Doppler Flowmetry.

This optical imaging technique measures CBF based on the Doppler frequency shift (blue) of backscattered light imparted by moving erythrocytes in cerebral vessels.

4.1.2 Technical Specifications

Flow imaging with Laser Doppler provides precise, real-time quantitative measurements of regional CBF and is distinguished by its superior **temporal** resolution (milliseconds), allowing to track rapid variations in flow. This feature is especially important for studying fast vascular responses to functional activation, e.g. subsequent to whisker or forepaw stimulation in rodents. However, because LDF is a single-point measurement technique, it offers little to no **spatial** information [138-140], and the measurements are restricted to a small sampling volume of 1 mm^3 which may not reflect the spatial heterogeneity of the cerebral microvasculature (e.g. capillaries vs. venules) adequately [141-143]. Whilst additional spatial resolution can be achieved with a scanning version of LDF [144], this is performed at the cost of a severely impaired temporal resolution (several seconds) due to time-consuming scanning, and thus is not recommended for the study of stimulation-induced changes in flow [145, 146].

Additionally, the penetration **depth** conferred by LDF is uncertain and is influenced by

tissue properties such as the vessels' structure and density, which alter the path length traveled by the photons irrespective of blood flow velocity. Hence, it is recommended when measuring cortical CBF that the fiber-optic probe be placed away from large superficial vessels, which would otherwise drastically reduce the attained depth [137, 147-149]. For imaging deep brain structures such as the hippocampus, a small corticostomy (~1.5 mm diameter) is performed so that the probe can be positioned at the desired location [150]. Penetration depth is also highly dependent on the wavelength of the emitted light, with infrared light penetrating deeper (several mm) than the blue and green light (0.15mm), and increases with the separation distance between the emitting and receiving fibers of the probe. Specifically, for near-infrared light (780 nm), penetration depth reaches approximately 0.5, 1 and 2 mm for separation distances of 0.125, 0.25 and 0.5 mm [151].

Compared with other imaging techniques, LDF is relatively easy to use, and the nature of the signal is well understood. In fact, the LDF signal clearly originates from the variations in flow velocity within the tissue being imaged. However, because the sensitivity of the probe to CBF is influenced by the distance between the tip of the probe and a particular vessel, the signal cannot be quantified in absolute units of CBF (e.g. mL/100g/min); rather, it is expressed as variations **relative** to a baseline value obtained under control conditions. Consequently, in order to be able to compare results from different experiments, the fiber-optic probe must be calibrated with specific motility standards, or an absolute measure of flux must be obtained through another method (e.g. quantitative autoradiography) [120, 152].

Moreover, one of the inherent limitations of this technique is its marked sensitivity to **motion** artifacts [120, 153]. This can result either from motion of the imaged tissue, or

movement of the fibers of the LDF probe. Fiber movement can be prevented by using an integrated probe which includes both the light emitting and receiving fibers [154-156]. Additional care should be taken during signal acquisition by placing the LDF setup away from vibrating instruments such as perfusion pumps, and by positioning the probe using a micromanipulator.

4.1.3 Applications in Awake Behaving studies

Since anesthesia greatly influences the animal's physiology, including cerebral autoregulation and the neurovascular response (see **Section 3**), many LDF systems have been proposed for imaging in the awake animal [69, 121, 132, 140, 157, 158]. In 1994, Sato's group recorded the regional CBF in conscious rats in response to inhalation of 7% Co2, by chronically attaching a LDF probe to the cortex and restraining the rat in a cloth hammock [157]. More recently, Takuwa and colleagues established a system for measuring CBF in conscious, freely moving mice, to enable the chronic investigation of CBF in a relatively natural environment [140]. In subsequent studies, the authors used this system to investigate the hemodynamic response in the awake, freely moving mouse during sensory stimulation [132] and neural deactivation [133]. Further, Tajima and colleague confirmed the reproducibility of CBF measurements in longitudinal studies using awake mice, using LDF at baseline, 1 hour later, and 7 days following the baseline measurement. In this study, the authors also improved the LDF system by stabilizing the fiber-optic probe on the cortex with a polyvinyl chloride tube, which is crucial for obtaining accurate measurements over extended recording sessions [158].

4.2 Laser Speckle Contrast Imaging (LSCI)

Another optical imaging technique commonly used for CBF monitoring is laser speckle contrast

imaging (LSCI), whereby a coherent laser light is projected onto an area of the skull or cerebral cortex. As the emitted light is scattered from different parts within the illuminated surface, it travels across distinct path lengths before being perceived by a photodetector (**Figure 7**). This variation in path lengths yields a constructive and destructive interference that changes with the positioning of the scattering particles, resulting in a randomly changing intensity pattern referred to as "**speckle**" [159]. In the brain, the movement of erythrocytes within blood vessels produces a time-varying speckle at each pixel in the image. Spatial variations in the speckle pattern can be plotted to produce two-dimensional maps of CBF, which show changes in flow velocity over time (**Figure 7**) [160].

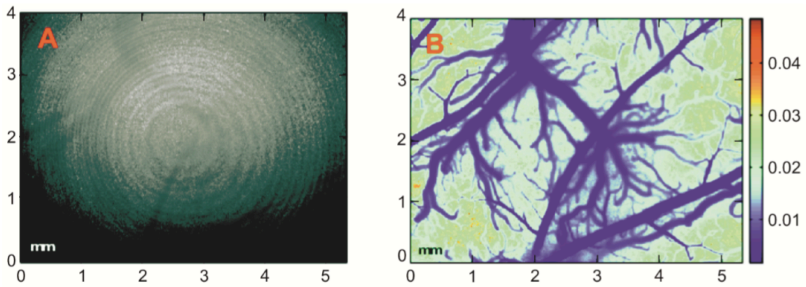

Figure 7. High resolution image of rat brain vasculature using laser speckle contrast.

Example of (a) a raw speckle image from the barrel cortex of a rat, and (b) its derived flow index map (figure reproduced from [115]).

Similarly to LDF, LSCI can be used to monitor CBF and functional activation in animal models with high **temporal** resolution (milliseconds). However, whilst the information obtained with LDF is **spatially** constrained, LSCI offers wide-field two-dimensional mapping of cortical CBF with excellent spatial resolution (~ 5-10 µm), allowing clear visualization of individual blood vessels [161, 162]. Similar high-resolution maps can be obtained using a laser Doppler scanner; however, this modality cannot compete with laser speckle on imaging speed. Indeed, a single Doppler scan requires several minutes to complete, whereas LSCI instruments enable full-field

imaging of CBF without requiring any scanning, and thus can be used to provide real-time images and even videos with some recent technologies. Nevertheless, parallel processing of the Doppler signals from each pixel, e.g. using on-chip processing, is being currently investigated by several groups as a means to enable the production of full-field images in real time [115, 163]. Once these techniques are fully developed and commercialized, laser Doppler scanners may become more popular than LSCI due to their inherently superior spatial resolution. However, the implementation of this approach would likely be very costly, and LSCI may still have room to compete by offering a relatively **inexpensive** and **easy-to-use** alternative [115].Moreover, whilst most of the current LSCI techniques require the use of anesthesia, several **miniature LSCI** imagers have been proposed to enable imaging of cortical CBF in the awake active rodent. These imagers are sufficiently small (~3 cm high) and lightweight (≤20 g) to be carried by the rat without hindering its movement, and offer similar spatiotemporal resolution compared with conventional LSCI systems [164, 165].

That said, LSCI shares many of the limitations described earlier for LDF (see **Section 4.1.2**). Indeed, due to the scattering nature of the cortical tissue, this technique also suffers from limited penetration depth and poor depth resolution, and thus can only be used to investigate vascular dynamics close to the cortical surface [166]. In addition, just like with LDF, the information obtained with LSCI cannot be expressed in **absolute** units. Moreover, LSCI does not permit rigorous **quantification** of CBF velocity, since the exact relation between the speckle contrast factor K and the flow velocity has yet to be determined [160]. Lastly, this technique is susceptible to **artifacts** which can be caused by variations in the parameters of the image acquisition system or in the optical characteristics of the imaging window. Hence, whilst LSCI is

a powerful tool for mapping CBF changes on the cortical surface, careful control of imaging parameters is warranted when comparing data from different imaging sessions [167].

4.3 Intrinsic Imaging

Intrinsic imaging techniques such as **optical imaging of intrinsic signals** (OIIS) and **two-dimensional optical imaging spectroscopy** (2D-OIS) are also frequently used to investigate cerebral hemodynamics [65, 168-181]. These approaches are based on the distinct optical absorption spectra of **oxyhemoglobin** (HbO) and **deoxyhemoglobin** (HbR) [31]. Because HbO is locally converted to HbR upon oxygen delivery to the neural tissues, the relative concentrations of HbO and HbR can be used to infer the blood's oxygenation levels and metabolic activity [112]. Hence, when the cortex is illuminated with laser light, active areas can be differentiated from inactive regions of the cortex based on a change in their optical reflectance and absorption properties, commonly known as **optical intrinsic signals**.

Intrinsic imaging offers several technical advantages over other imaging modalities. Indeed, the spatial resolution of OIIS is very high relative to other experimental imaging techniques, making it ideally suited for the study of NVC at the level of arterioles, capillaries and veins. As such, this technique can determine patterns of cerebral hemodynamics over large areas of the cortex (~25 mm^2) with **a spatial** resolution up to 50µm and high **temporal** resolution (~100 ms) [169, 175, 182-184]. As with LDF and LSCI (see **Sections 4.1.3** & **4.2**), the depth of optical maps is determined by the wavelength of the laser light that is used to illuminate the cortex, with visible light detecting change at a maximum depth of 1 mm [185] and near-infrared light reaching up to 2 cm below the pial surface [186, 187]. Further, since intrinsic imaging does not necessitate contact with the cortical surface or the use of potentially phototoxic dyes (as

with extrinsic imaging techniques), it is minimally invasive and thus has been applied to imaging studies in awake, freely moving monkeys [188], cats [189], rats [180, 190] and mice [191].

The real power of intrinsic imaging stems from its ability to measure changes in blood volume, oxygenation or light scatter, according to the chosen wavelength of laser light [176, 192, 193]. That said, a major problem with the intrinsic method is that the motion-induced **noise** and vascular **artifacts** associated with intrinsic signals are often of similar or larger magnitude than the signals themselves [194-196]. As such, it is critical to minimize motion by ensuring complete head stabilization of the imaged subject. Interestingly, the choice of wavelength has been shown to influence the presence of vascular artifacts, with orange light offering the best signal to noise ratio in the visual cortex [197], and green light in the auditory cortex [198].

4.4 Two-Photon Laser Scanning Microscopy (TPLSM)

The aforementioned imaging modalities (LDF, LSCI & IOS) have greatly enhanced our knowledge of cerebral hemodynamics, by allowing to image broad changes in blood flow, volume and oxygenation. TPLSM complements these techniques by enabling a systematic analysis of cerebral hemodynamics at the level of individual microvessels, in conjunction with simultaneous measurements of neuronal and glial activity. Moreover, the deep red and infrared light used with TPLSM can penetrate deep into the tissue, reaching up to 1 mm in **depth**, or in the cm range when using **gradient index lenses** directly into the cortex from a hole in the skull [199-201]. Since its invention, this modality has been used extensively to image cerebrovascular dynamics in *in vitro* [42, 202-206] and *in vivo* [207-213].

With TPLSM, a laser beam is focused through an objective lens and onto a micrometers-sized area within a specimen, in order to excite fluorescent molecules (fluophores) [214]. When

the excited fluophore reverts to its ground state, a photon is emitted and the emission light is captured by the objective, thus yielding an image of the fluorescent structures within the biological sample [215-217]. Two complementary parameters, **vessel diameter** and **RBC velocity**, are used to assess the hemodynamics of cerebral vessels. To measure these parameters *in vivo*, the plasma is labelled with an intravenous bolus of space-occupying high-contrast molecules, such as **dextran-conjugated fluorescent dyes** (e.g. fluorescein isothiocyanate) [218]. This enables the visualization of hemoglobins as dark shadows against a bright fluorescent background.

Notably, TPLSM can be used in conjunction with **anatomical** markers such as traditional dyes and functional markers, in order to enable real-time monitoring of specific structural dynamics (e.g. cellular morphology or protein localization). Moreover, the use of **functional** markers such as voltage-sensitive fluorescent dyes and fluorescent ion indicators, can provide simultaneous recordings of the activity of neurons, glias and VSMCs [204-206, 210, 219]. This is important since it can allow to determine the complimentary roles of these cells in initiating NVC under physiological conditions, and the mechanisms that lead to its dysfunction in different pathologies. Lastly, the recent development of **miniaturized**, head-mounted two-photon microscopes has opened the door to two-photon imaging in the awake, freely moving animal [220].

That said, whilst TPLSM provides superior spatial resolution, allowing to visualize individual microvessels and subcellular compartments, the imaging of vascular dynamics and cellular activity is limited to vessels and cells that are closely associated and lie in the same imaging plane. This is problematic since somatosensory-evoked NVC extends laterally across

the brain surface and deep into the cortex, and is associated with significant trial to trial variability [57, 221]. Nevertheless, this limitation has been recently overcome with the advent of volumetric imaging, which utilizes an elongated, V-shaped point spread function to visualize a three-dimensional brain volume [222].

4.5 Multimodal imaging and Optogenetics

All in all, optical imaging techniques utilize the optical properties of the imaged tissue such as reflectance, scattering and fluorescence, in order to produce image contrast. In section, we have described different optical imaging systems, including laser Doppler, laser speckle, intrinsic imaging and TPLSM, each of which has contributed significantly to our current understanding of the cerebral vasculature and the hemodynamic response. Since these techniques have been developed based on different concepts, they are distinguished in terms of spatial resolution, temporal resolution, depth penetration as well as the nature of the information they provide (**Table 1**). Hence, whilst LDF and LSCI provide excellent temporal resolution, intrinsic methods present greater versatility since they allow to track several vascular parameters (CBF, CBV and oxygenation). Further, all three aforementioned systems, along with macroscopic imaging techniques (e.g. fMRI, PET and NIRS) allow to visualize broad changes in cerebral hemodynamics, whereas TPLSM conveys microscopic information regarding single capillary flow and subcellular dynamics. Therefore, different imaging modalities can be combined in order to yield complimentary information about the cerebral vasculature, as has been done by many research groups [223-231]. For example, Ringuette and colleagues recently investigated the relationship between regional CBF, oxygen saturation and intracellular Ca^{2+} dynamics using three different optical imaging systems (LSCI, OIS and Ca^{2+}-sensitive dye imaging) [230]. In

another recent study, Takuwa et al. developed a multimodal imaging system for simultaneous measurement of CBF by LSCI and PET in awake behaving mice [231].

Furthermore, optical imaging can be combined with optogenetic techniques to manipulate cell-specific vasoactive signaling cascades *in vivo*. Indeed, several transgenic mouse lines have been developed with cell-type specific expression of light-gated ion channels or pumps of bacterial origin, such as channelrhodopsin-2 (ChR2) and halorhodopsin. These genetically encoded optical actuators can be activated using specific laser wavelengths (e.g. blue-green light for ChR2 or yellow for halorhodopsin), leading to activation of cells that express the transgene [232, 233]. Hence, optogenetics can be used to investigate the specific neuronal subtypes and neurotransmitters that are involved in the initiation of the vasodilatory or vasoconstrictive responses during functional hyperemia. However, to ensure cell specificity, measures must be taken in order to inhibit the spread of depolarization to other cell types. For instance, unless synaptic communication is prevented, photoactivation of pyramidal cells elicits connectivity between different brain areas, leading to the firing of several cellular types and the release of many neurotransmitters [34, 234]. Moreover, Rungta and colleagues have recently found light *per se* to cause a Ca^{2+} decrease in VSMCs and to induce vasodilation, independently of neural and glial activity, thus warranting the careful use of optogenetics in studies involving the cerebral circulation [235].

5. Implications of Stress in Conscious Imaging

5.1 Effect of Stress on Cerebral Hemodynamics

One concern that arises when performing imaging in conscious animals is that they may experience high levels of stress due to head immobilization or the imaging procedure itself. As we will see, stress has been shown to produce systematic effects on the brain and to induce variations in CBF, CMR and NVC through effects on neuronal and glial populations as well as the cerebrovascular system.

Indeed, in an early review by Kety and colleagues, it was observed that one human participant who had showed considerable fear throughout the test situation exhibited markedly elevated CMR of oxygen (**$CMRO_2$**) (5.0 mL/100 g/min) relative to his physiological range (3.2-4.2 mL/100 g/min) [236]. The authors concluded that apprehension or stress could lead to increases in cerebral metabolism. Similarly, another study in humans showed pain-induced stress to increase **CBF** by approximately 10%, especially in frontal brain regions [237]. These clinical observations were replicated experimentally with rats, with 5 to 30 minutes of immobilization with a muscle relaxant inducing up to twofold increases in both CBF and $CMRO_2$ [238, 239]. Additional stressors that were found to increase CBF and CMR in laboratory animals include ethanol withdrawal [240, 241], hypotension [242], hypoxia [243, 244] and conditioned fear [245, 246]. In contrast to pharmacological immobilization and the aforementioned stressors, Ohata and colleagues found physical immobilization (5-15 minutes) to *decrease* CBF by ~12-14% in wild type rats [247], and to have no effect on CBF in spontaneously hypertensive rats except in the frontal lobe where flow was increased by 21% [248]. However, in the latter studies, the restraint procedure elicited hyperventilation in the rats, leading to a significant decrease in the levels of

vasodilatory CO_2. Hence, the resulting constriction of cerebral vessels could have offset stress-evoked increases in CBF or led to reduced flow. Interestingly, tissue lactate was reported to increase during physical restraint [249], reflecting an increase in **CMRglc**. These findings suggest that restraint stress increases metabolic demands in the brain, though these changes may not always be accompanied by an increase in CBF, due to altered cerebral hemodynamics.

Indeed, chronic immobilization (2 hours per day, for 10 consecutive days) was found to attenuate changes in CBF in the rat somatosensory cortex of following inhalation of high amounts of CO2 [250]. Similarly, chronic immobilization (2 hours per day, 3 weeks) diminished the cerebrovascular response to electrical stimulation of the rat hindpaw, as observed by the reduced variations in CBV and pial arterial dilatations relative to the control condition. Moreover, when rats were subjected to varying lengths of immobilization stress, the hemodynamic response was the least decreased in the acute restraint group (2 hours, single session), and the most decreased in the chronic 6-week restraint group, suggesting that stress exerts cumulative effects on **NVC** [251].

5.2 Stress-induced Modulation of the Neurovascular Unit

As with anesthesia-evoked NVC impairment (**see Section 3.1**), stress induction in conscious animals likely interferes with cerebral hemodynamics by effecting changes in neural, vascular and glial cells. Indeed, chronic stress exposure has been demonstrated to influence the physiology of **neurons** and to elicit detectable microscopic changes in neuronal networks involved in the processing of anxiogenic and fearful stimuli. Specifically, changes include the modulation of the dendritic arborization, spine and synapse count in the amygdala, the hippocampus and the prefrontal cortex [252]. These stress-induced structural changes are partly

caused by alterations in the expression of various stress-related proteins, such as tissue plasminogen activator [253], stress-related proteins (e.g. corticotropin-releasing factor) [254] and neural adhesion molecules [255].

Whilst most of the research conducted on the effects of stress in the CNS has been focused on neurons, studies increasing show glial and vascular cells to also be affected. Indeed, chronic stress is detrimental to the proliferation and survival of **glial cells**, particularly in the limbic brain structures. In humans, long term treatment with high dose steroids, which are elevated during stress, is associated with a considerable reduction in the number and density of glial cells in fronto-limbic regions of the brain [256]. Similarly, animal models of chronic stress demonstrate reduced gliogenesis in limbic regions [257], and administration of a synthetic glucocorticoid (dexamethasone) *in vitro* selectively abrogates astrocytic differentiation from neural precursor cells [258]. Functionally, **astrocytes** express both glucocorticoid and noradrenergic receptors, and thus constitute direct targets of stress hormone actions [259]. Addition of glucocorticoid to astrocytic cell cultures has been shown to interfere with glutamate clearance [260] and to amplify the amplitude and propagation of astrocytic Ca^{2+} waves two-fold compared with controls [261], possibly leading to enhanced communication with other cells. Like glucocorticoids, norepinephrine is also greatly increased during stress and has been shown to increase astrocytic Ca^{2+} signaling [262] and to interfere with astrocytic glycogenolysis and glutamine uptake [263] by binding noradrenergic receptors on astrocytes. Moreover, Chatterjee and colleagues found that addition of high levels of corticosterone (100 nM and 1 μM for 3 hours) to cultured astrocytes, which generates stress-like conditions, increased the release of vesicles containing pro-atrial natriuretic peptides (ANP) from astrocytes by altering their cytoskeletal

arrangement. Since ANP exerts downstream actions on both neural and vascular cells, influencing its release could produce alterations in NVC under stress-associated pathological conditions [264]. In addition to modulating astrocytic function, chronic restraint stress in mice [265] and rats [266] was also found to enhance microglial proliferation and ramification in the amygdala and hippocampus. Chronic activation of **microglia** is known to enhance inflammation through the release of cytokines such as IL-1β, IL-6, and TNF-α [267] and is thus expected to further exacerbate the stress-evoked alterations in cerebral hemodynamics.

Notably, prior to reaching neurons, astrocytes and microglia, stress hormones travel across the cerebral vasculature, where they may activate glucocorticoid receptors expressed on brain ECs and VSMCs [268, 269]. Indeed, Longden and colleagues found that subcutaneous delivery of corticosterone (2.5 mg/kg, daily for 7 days) in rats reduced the number of functional inwardly rectifying K^+ channels in the myocyte membrane, which is expected to decrease arteriolar sensitivity to K^+ released by astrocytes and thus impair K^+-mediated vasodilation during the hemodynamic response. Accordingly, the authors reported a decrease in the vasodilatory response to electrical field stimulation by 43% [3]. The resulting suboptimal vasodilation could reduce the amount of blood delivered to active brain regions, thereby leading to compromised NVC and functional hypoperfusion in stressed animals.

Aims and Hypothesis

In the present thesis, our **general aim** was to develop an awake imaging model which would enable the study of NVC in the conscious, head-restrained mouse, whilst overcoming the effects of anesthesia and stress on the cerebral vasculature. For this purpose, we sought to meet three specific objectives.

Our first objective was to build a simple, cost-effective **restraint apparatus** which would immobilize the mouse's head in order to prevent motion-induced noise artifacts during imaging sessions, whilst leaving the mouse free to run, walk or self-groom. In particular, the restraint apparatus ought to be easily adjustable according to each mouse's size, in order to allow for natural movement and maximize the level of comfort. We also wanted the apparatus to be compatible with several optical imaging modalities frequently used to study NVC, including laser Doppler, laser Speckle, intrinsic imaging and two-photon microscopy.

Our second objective was to create a brief yet effective **training regime** which would acclimate the mice to head restraint in preparation for the imaging sessions. Indeed, in previous awake imaging studies, animals have been gradually accustomed to head restraint over a habituation period which can vary from a single day up to several weeks [83, 270-276]. Importantly, the training regime should enable the mice to tolerate head restraint, whilst minimizing the level of stress and the amount of movement during the imaging sessions.

For our third objective, we sought to establish a protocol for the **quantitative evaluation of stress levels** in mice. Typically, the animal's adaptation to the restraint procedure is assessed visually through careful observation of the animal's vocalizations, movement and exploratory

behavior. However, few awake imaging studies to date have resorted to a quantitative measure of stress. In our study, we chose to measure the evolution of corticosterone levels in mice prior to and throughout the habituation period, in order to probe the effectiveness of our training regimen in reducing stress.

Our **hypothesis** was that, by exposing mice to several sessions of head restraint, we would gradually reduce the stress that is associated with head restraint, as reflected by a decrease in plasma corticosterone levels. Ultimately, we would have developed a novel imaging model with a habituation protocol which would allow to study a hemodynamic response that is unadulterated by the effects of anesthetics and stress, thereby facilitating the translation of cerebral hemodynamics from mice to humans.

Methods

Animals

Two to three months old C57BL/6J mice (Jackson Laboratory, Canada) were housed individually in a temperature-controlled room (22˚C) and kept under a 12-hour light/dark cycle. All animal procedures were approved by the institutional Animal Care and Use Committee of Université de Montréal and performed in accordance with the guidelines of the Canadian Council for animal care.

Main Procedures

1. Development of a Custom-Made Restraint Apparatus

The **traditional stereotaxic apparatus** used to immobilize the anesthetized mouse's head would cause great discomfort to the conscious mouse and thus is not suitable for use in awake studies. Consequently, we have custom-built two different restraint devices aimed at immobilizing the awake mouse during imaging sessions (see **Figure 8**), in collaboration with Mohammad Moeini and Samuel Bélanger in Dr. Lesage's Laboratory (École Polytechnique de Montréal, QC, Canada).

Our first device consisted in **a full-body restraint apparatus**, the components of which were initially designed by software (Autodesk), then built with a three-dimensional printer and assembled together using screws. This device was developed based on the design of the traditional stereotaxic device, in that it also included a **tooth holder** to help adjust the positioning of the rodent's head, and a **nose cone**, to enable the delivery of gas anesthetics when

required. A few adjustments were made to better suit the awake animal. For instance, the ear bars of the traditional stereotax, which would be too painful for the awake mouse, were replaced with a **head piece** which would similarly allow to immobilize the head, whilst exposing the cortex for optical imaging. We also built a larger **body piece** to be positioned on top of the mouse, for full-body restraint. Since the device components were easily detachable and replaceable, they could be tweaked separately in order to further reduce body movement whilst minimizing the discomfort of the restrained animal.

Nevertheless, in order to further reduce the stress and discomfort associated with forced immobilization during prolonged imaging sessions, we proceeded to assemble a second restraining device, where only the animal's head would be immobilized, and its body would be free to move. Specifically, this **head-restraint device** comprised an inclined wheel, on which the mouse could walk, run or rest. The wheel was built using a three-dimensional printer, and was set at an angle (rather than horizontally) in order to encourage the mice to run and thus prevent them from falling asleep during prolonged imaging sessions. The wheel was fixed atop of an **aluminum platform** and opposite of a horizontal **headpost**, to which the mouse's head would be attached by the means of a head bar and two screws (4–40 screws, McMaster Carr, Aurora, OH, Canada). Both the headpost and the wheel could be adjusted to accommodate for the animal's size and comfort. The parts that were used to build this apparatus are listed in **Table 2**.

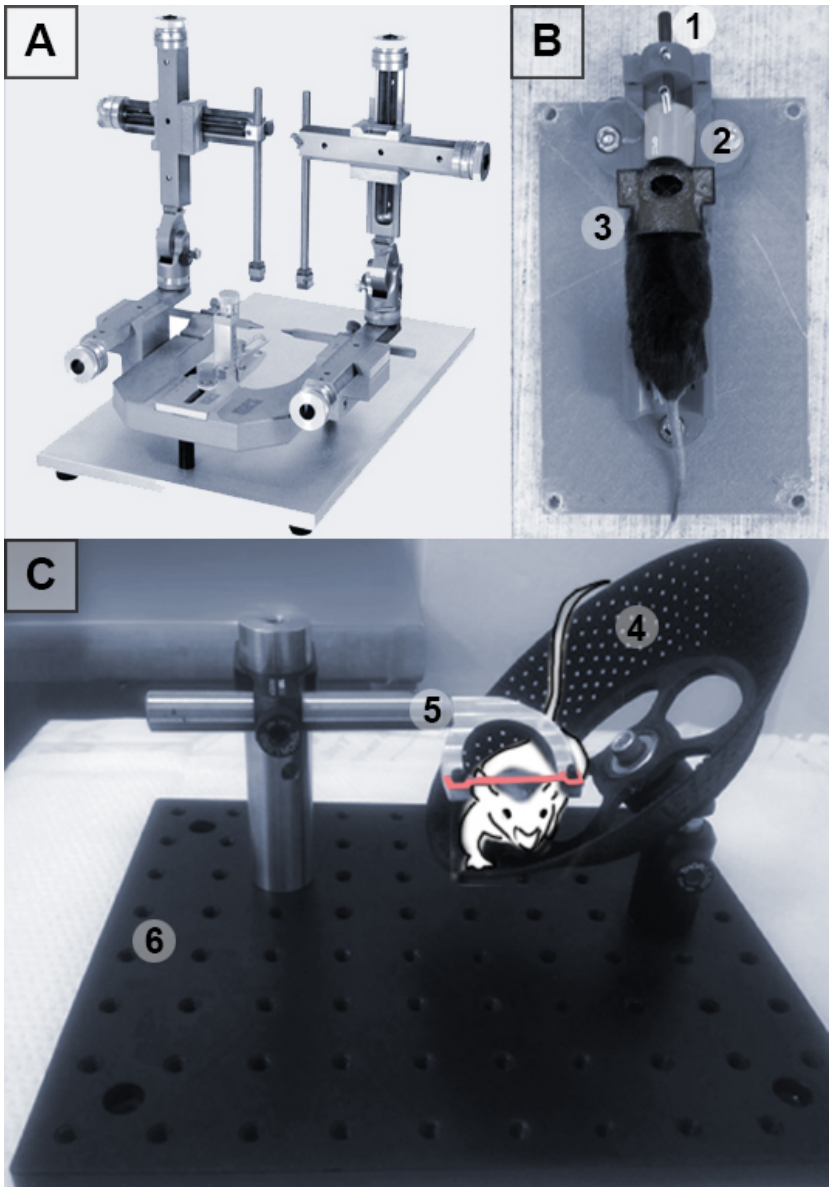

Figure 8. Development of a Restraint Apparatus for Conscious Imaging in Mice.

(A) Image of a traditional stereotax, used with anesthetized mice. (B) Full-body restraint apparatus, where the mouse was immobilized with a tooth bar (1), nose cone (2), head piece (3) and body piece (not shown). All the pieces were created with a three-dimensional printer and easily assembled and de-assembled using screws. Immobilization with this device required prior anesthesia with isoflurane. (C) Head-restraint apparatus, which comprised an inclined wheel (4) and a horizontal headpost (5), affixed opposite of each other on an aluminum platform (6). The conscious mouse (colored in white for visibility) was gently placed on the wheel and its head bar (colored in red) was quickly attached to the headpost by the means of screws. The position of the headpost and wheel was then adjusted according to the mouse's size and comfort.

Table 2. List of the parts used for building the head-restrained device.

Quantity	Description	Vendor	Part Number	Price
1	Rolling blade bearing	-	-	$10.00
1	Breadboard	ThorLabs	MB2025/M	$110.00
1	25 mm Post, L = 100 mm	ThorLabs	RS100/M	$26.00
1	Right-Angle 25.0 mm to ½ " Post Clamp	ThorLabs	RA90RS/M	$25.50
1	12.7 mm Optical Post, SS, M4 Setscrew, M6 Tap, L = 40 mm	ThorLabs	TR40/M	$4.90
1	12.7 mm Post Holder, Spring-Loaded Hex-Locking Thumbscrew, L = 40 mm	ThorLabs	PH40/M	$7.22
1	Mounting Adapter	ThorLabs	MA45-50/M	$20.60

2. Head Bar Installation Surgery

2.1 Head Bars

Titanium head bars were custom-made by Lesage Laboratory according to a design provided by Tran and Gordon [276] (see **Figure 9**), to be later installed onto the mouse's skull during a brief surgical procedure. The head bars were to be attached to the horizontal head post of the head-restraint apparatus during habituation and imaging sessions, in order to immobilize the animal's head.

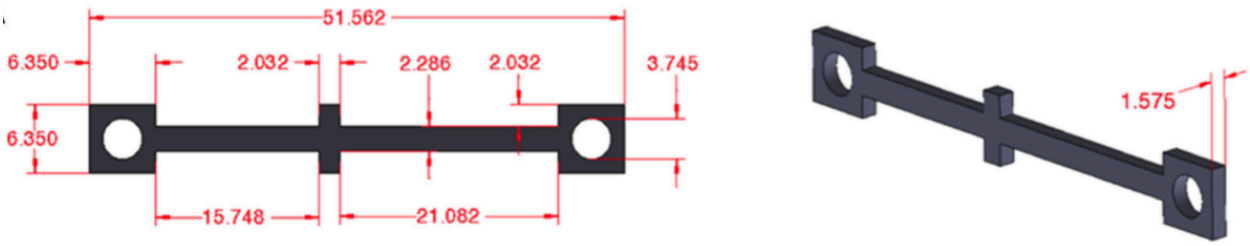

Figure 9. Dimensions (in mm) of the custom-made titanium head bar.

(Figure adapted from [276]).

2.2 Anesthesia Induction

The mouse was placed inside of a closed induction chamber, and anesthesia was induced with a mixture of 4% isoflurane and 3 L/min oxygen. Next, the mouse was moved to a stereotaxic apparatus and the anesthesia was maintained with 2% isoflurane and 1.5 L/min throughout the surgical procedure, which lasted approximately 15 minutes. The depth of anesthesia was monitored by observing the animal's breathing rate and testing motor responses to tail and toe pinches, and the body temperature was measured by a rectal probe and maintained at 37˚C using a controlled heating pad (TCAT-2, Physitemp Instruments).

2.3 Surgical Procedure

All surgical instruments were sterilized with a dry bead sterilization unit (Germinator 500, Braintree Scientific, USA) prior to surgery. The procedure was performed as previously described [276-278]. Following anesthesia induction, a sterile ophthalmic gel was applied to protect the eyes from irritation or dehydration. The mouse was administered with Tribrissen (30 mg/kg) and Carprofen (5 mg/kg) through subcutaneous injection into the right and left hindpaws, to prevent post-surgical infection and inflammation, respectively. The skin on top of the head was shaved, cleaned with three alternating swabs of 70% ethanol and iodine and numbed via subcutaneous injection of a local anesthetic (Marcaine, 2m4 mg/kg). After a 3-minute wait (the time for the skin to become numb), an incision approximately 3 cm in length was performed across the midline of the brain with a pair of surgical scissors, and the two flaps of skin were removed, exposing the skull from the nasal bone down to the interparietal bone. The periosteum (vascular connective tissue) was then scraped off with a scalpel, and the skull was dried with gauze. Next, the skull was covered with a thin layer of tissue adhesive (3M

Vetdbond™, USA) along with the temporalis muscle and wound margins, whilst avoiding the left somatosensory cortex and surrounding skin. The tissue adhesive prevented the seepage of the serosanguinous fluid and enhanced the adhesion of the dental cement to the bone. Once the tissue adhesive had dried, a thin layer of dental cement was applied to the skull. The titanium bar was then positioned on the interparietal bone and glued in place by applying several coats of dental cement on top of the skull and the titanium bar, whilst taking great care to leave the left somatosensory cortex exposed for subsequent optical imaging (see **Figure 10**). Once the dental cement had cured, anesthesia was discontinued and the animal was placed in an individual, clean cage.

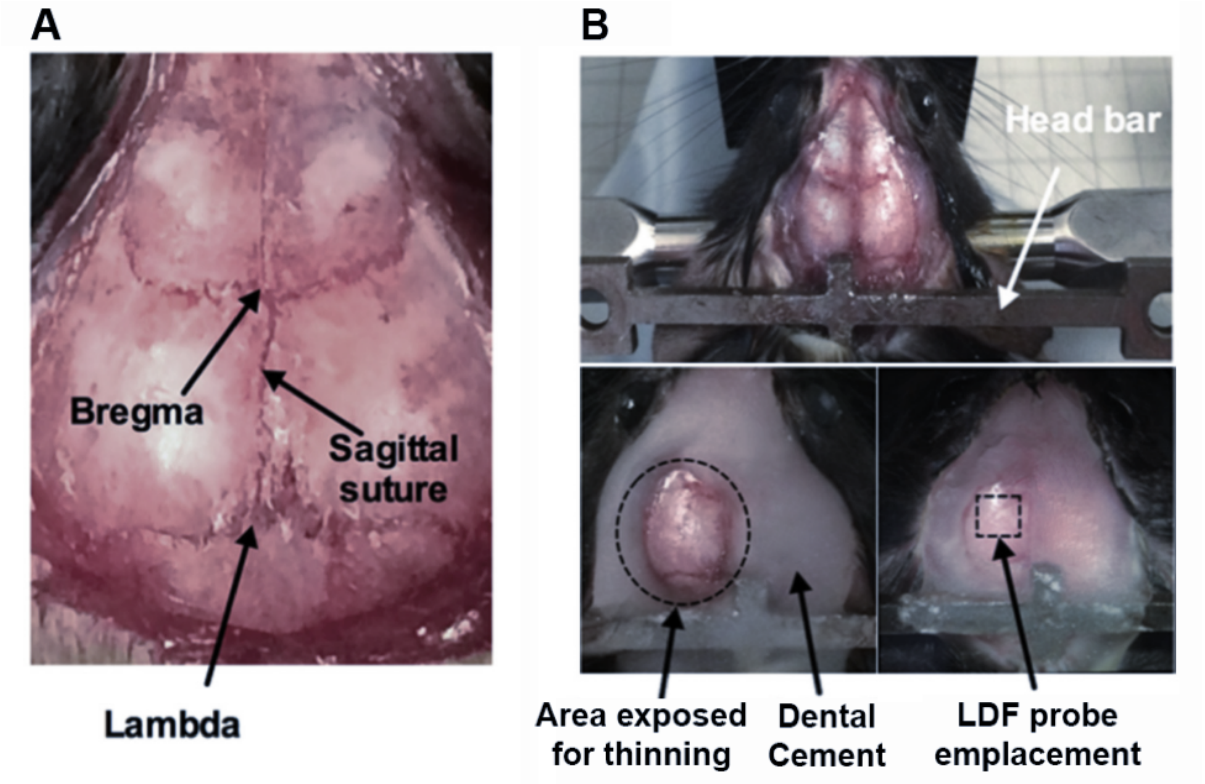

Figure 10. Head bar installation surgery.

(A) Top view of the mouse's skull, with the periosteum scraped off with a scalpel blade, showing bregma, lambda and the sagittal suture. (B) A thin layer of Vetbond tissue adhesive was applied over the skull (top), followed by several layers of dental cement (bottom). The head bar was installed behind lambda, over the interparietal bone, and the left somatosensory cortex was left unexposed for subsequent bone thinning and optical imaging with laser Doppler (Figure modified from [276]).

2.3 Postoperative Care

A daily dose of Tribrissen (30 mg/kg) and Carprofen (5 mg/kg) was administered during the following two days (or longer when required, e.g. in the event of an infection). Throughout the remainder of the experiment, the mice were frequently weighed and monitored for signs of pain or discomfort.

3. Acclimation to Head Restraint

The mice were gradually acclimated to head restraint using a three-step approach: handling, exposure to the wheel and head restraint. On the first two days of habituation, the mice were handled by gently placing them into the palm of the hands for 10 minutes or until grooming behavior was observed, in order to habituate them to the experimenter. Notably, to eliminate potential confounds, all behavioral experiments in mice were performed by the same experimenter. On the third day, the animals were placed on the inclined wheel without restraint, and were left to run, walk, rest or groom on the wheel for 10 minutes. For the remainder of the habituation protocol, each mouse was sequentially attached to the wheel for a daily session of predetermined duration.

4. Bone thinning

Prior to the optical imaging session, a 2x2 mm^2 area of the overlying skull was thinned to translucency in order to gain visual access to the mouse left somatosensory cortex. The drilling was performed using a dental drill with a 0.6 mm burr at a 30˚C angle and in all directions (using horizontal, vertical and diagonal strokes) as to yield a smooth surface. The bone was frequently cooled with saline in between drillings to prevent overheating the dura matter and brain tissue.

A small amount of controlled bleeding was observed from the vessels in the inner cancellous layer of the bone, and was easily stopped by applying light pressure with a cotton swab. The thinning was considered sufficient when the vasculature became clearly visible after applying a drop of saline solution.

5. Laser Doppler flowmetry

Variations in CBF were continuously monitored by LDF. The optic probe was positioned stereotaxically on top of the thinned skull and perpendicular to the surface of the cortex, and was connected to a computerized data acquisition system. The positioning of the probe was further adjusted by screening the hemodynamic response within the somatosensory cortex, whilst taking care to avoid large blood vessels. The lights were then turned off, and the mouse was left alone for thirty minutes, in order for the CBF to stabilize. Next, the hemodynamic response was elicited by gently stroking the right whiskers (4-5 Hz) with a cotton swab continuously for three sessions of 60 seconds each, interspaced by 60 seconds of rest. Data was smoothed at 303, and the magnitude of CBF increases during whisker stimulation was calculated as percent changes relative to baseline over a period of 5 seconds, using LabChart 8 software. Zero values of CBF were acquired following cardiac arrest induced with an overdose of isoflurane at the termination of the experiment. Since the main purpose of the present study was to analyze the stress levels associated with awake imaging in mice, we have only collected preliminary values for CBF.

6. Corticosterone ELISA

A corticosterone enzyme-linked immunosorbent assay (ELISA) (ADI-900-097, Enzo Life Sciences, USA) was performed in order to track variations in stress during the habituation

period. The minimum corticosterone detection level of the ELISA kit was 26.99 pg/mL. Blood samples were taken between 9:00 am and 12:00pm, as to minimize the effect of the circadian rhythm on glucocortiocoid levels [279]. The blood was collected into a heparinized centrifuge tube, either from the facial vein of the conscious mouse (~8 µl blood) by piercing the cheek with a 26-gauge needle, or from the trunk following decapitation (~ 1 mL blood), and was immediately fractioned by centrifugation (2000 rcf, 4˚C, 20 minutes) to separate the plasma from other blood components. The plasma was then aspired with a micropipette and stored in a different tube at -20˚C. Once all the desired plasma samples were collected, they were diluted 1:20 and an ELISA was performed to determine the corticosterone levels in each sample.

Briefly, 100 µL of plasma or standards was added in duplicates to the wells of the microtiter plate, and 150 µL of assay buffer was added to the non-specific binding wells. Next, 50 µL of blue conjugate was added to each well except the blank well, and 50 µL of yellow antibody was added to all wells except the blank and non-specific binding wells. The plate was shaken (500 rpm) for 2 hours at room temperature, after which it was rinsed with a wash solution and emptied on absorbent paper. Subsequently, 200 µL of the substrate was added to each well and was incubated for one hour at room temperature. The reaction was terminated with 50 µL of stop solution per well. The optical density of corticosterone was scanned at 405 nm wavelength using a microplate luminescence reader and the corticosterone levels were determined from the standard curves.

7. Experimental Series

Three separate experimental series were conducted to test our hypothesis (see **Results**). For each series, we adjusted the experimental conditions, the habituation protocol and the blood collection method, depending on the literature and the obtained results.

8. Statistical Analyses

Data were expressed as means ± standard deviation of the mean. Differences in corticosterone levels (ng/mL) between blood plasma samples were examined with IBM SPSS 23.0 software using a **one-way analysis of variance** (ANOVA). If the results were significant, the intergroup variation was measured by **Tukey's multiple comparisons test**. Results were considered significant if $p < 0.05$.

Results

1. Laser Doppler flowmetry

Preliminary measures for CBF were performed over three sessions of whisker stimulation, in an awake and an anesthetized mouse. We found the hemodynamic response to be twice as large in the awake mouse, relative to the anesthetized animal (see **Figure 11**). Moreover, the awake animal presented fewer CBF fluctuations and artifacts at rest, and a more consistent response to whisker stimulation (see **Figures 12, 13**).

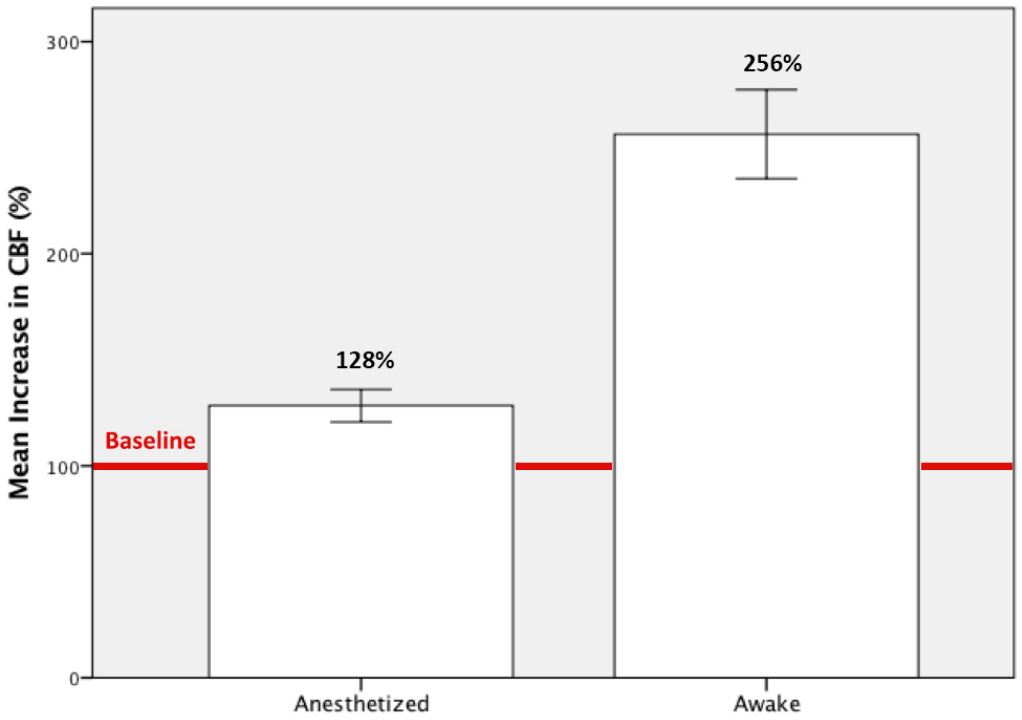

Figure 11. Hemodynamic response to whisker stimulation in the anesthetized and awake mouse.

CBF was measured in the left somatosensory cortex of one anesthetized and one awake mouse. The mean increase in CBF following stimulation of the right vibrissae was estimated as an average increase (%) following three whisker stimulation sessions, relative to the baseline state (red line).

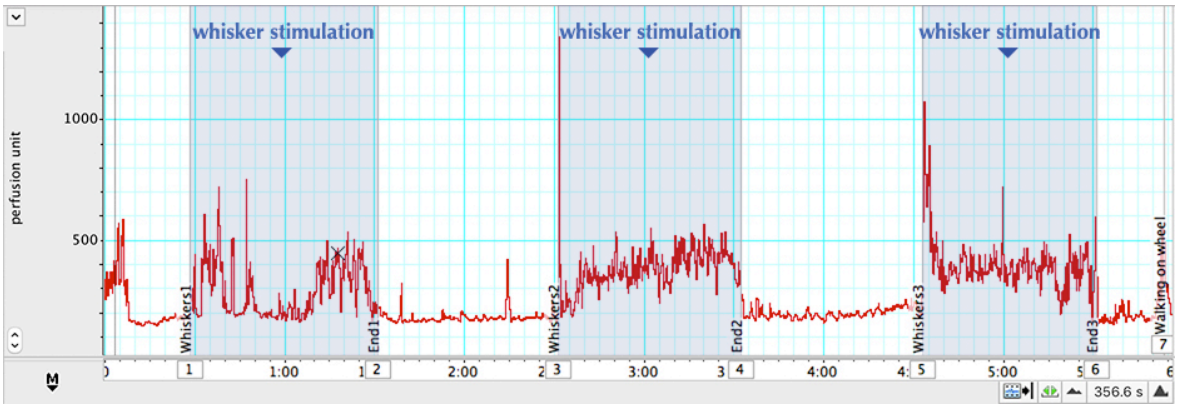

Figure 12. Hemodynamic response to sensory stimulation in the awake behaving mouse.

LDF chart showing variations in cerebral perfusion (x axis; arbitrary units) as a function of time (y axis; seconds). Variations in CBF were measured with LDF at baseline (no stimulation), and following three sessions of whisker stimulation (highlighted in blue). All measurements were performed in the left somatosensory cortex of the same awake behaving mouse.

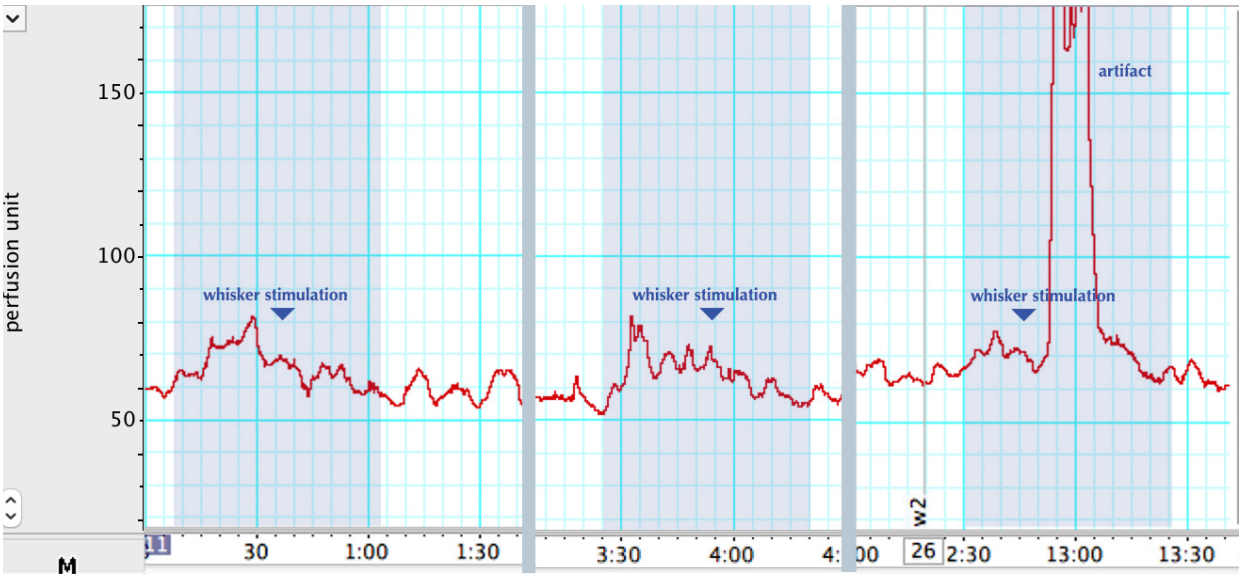

Figure 13. Hemodynamic response to sensory stimulation in the anesthetized mouse.

LDF chart showing variations in cerebral perfusion (x axis; arbitrary units) as a function of time (y axis; seconds). Variations in CBF were measured with LDF at baseline (no stimulation), and following stimulation of the right vibrissae (highlighted in blue). All measurements were performed in the left somatosensory cortex of the same anesthetized mouse.

2. Corticosterone ELISA

Experimental Series 1

Experimental Design

The first experimental series followed a **within-subject design**, where the variations in corticosterone levels across different experimental conditions were measured in mice (n = 7) using repeated blood collection from the facial vein (see **Figure 14**).

In order to habituate the mice to the experimenter, the rodents were each **handled** daily (from day 1 to day 5) by placing them on the palm of the hands until they initiated grooming behavior (5-10 minutes). The **head bar installation surgery** was performed on day 4, and the mouse was left to explore and run on the wheel the next day for 10 minutes without any restraint.

From day 6 until day 12, the mouse was restrained on the wheel for sessions which were gradually increased in length by 10-minute increments. On day 14, the mice were moved from the animal facility to the surgery room which contained the equipment required for optical imaging. The animal was gently attached to the wheel, its skull was thinned and the hemodynamic response was assessed using LDF. In order to evaluate the variations in stress levels throughout the acclimation period, we collected blood from the **facial vein** before the mice were exposed to the wheel as a **baseline value** (day 3), during **habituation to head restraint** (days 6, 9 and 12) and subsequent to LDF **imaging** (day 14). Upon termination of the experiment (day 14), blood was also collected from the mouse trunk following decapitation. We expected plasma corticosterone levels to reach their peak on the first day of head restraint (day 6), and to decrease significantly by the end of the experiment (days 12 and 14), thus reflecting a reduction in the stress experienced by mice following habituation sessions.

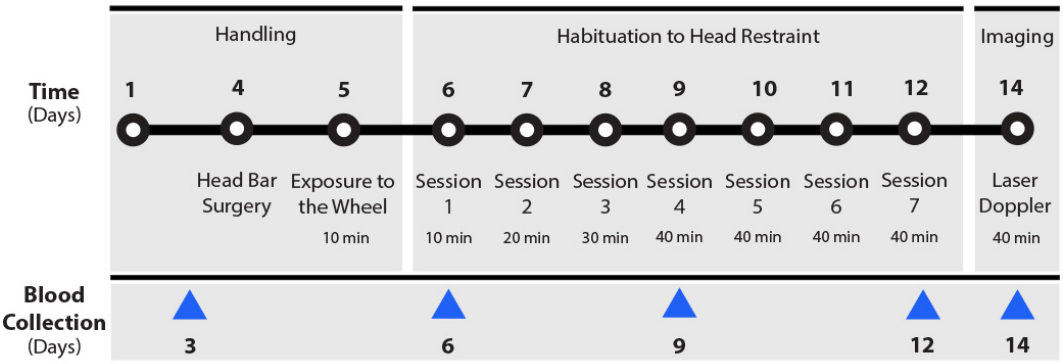

Figure 14. Protocol summary for habituation and blood collection in the first experimental series.

Mice (n = 7) were gradually acclimated to head restraint using a three-step approach: handling, exposure to the wheel and head restraint. Blood was collected from each mouse on several days (indicated by blue triangles) in order to determine the variations in corticosterone levels.

Findings

There was a statistically significant difference as revealed by one-way ANOVA (F (5,32) = 6.492, p = 0.000). The Tukey multiple comparisons test determined corticosterone levels (ng/mL) to be lowest following gentle handling (**34.22** ± 9.21), after which they were significantly increased by at least a factor of 10 ($p < 0.05$). The habituation sessions had no significant effect on corticosterone levels ($p > 0.05$) (**Figure 15**, possibly due to the prolonged duration of the restraint sessions, or to the cumulative stress associated with repeated puncturing of the facial vein for blood collection.

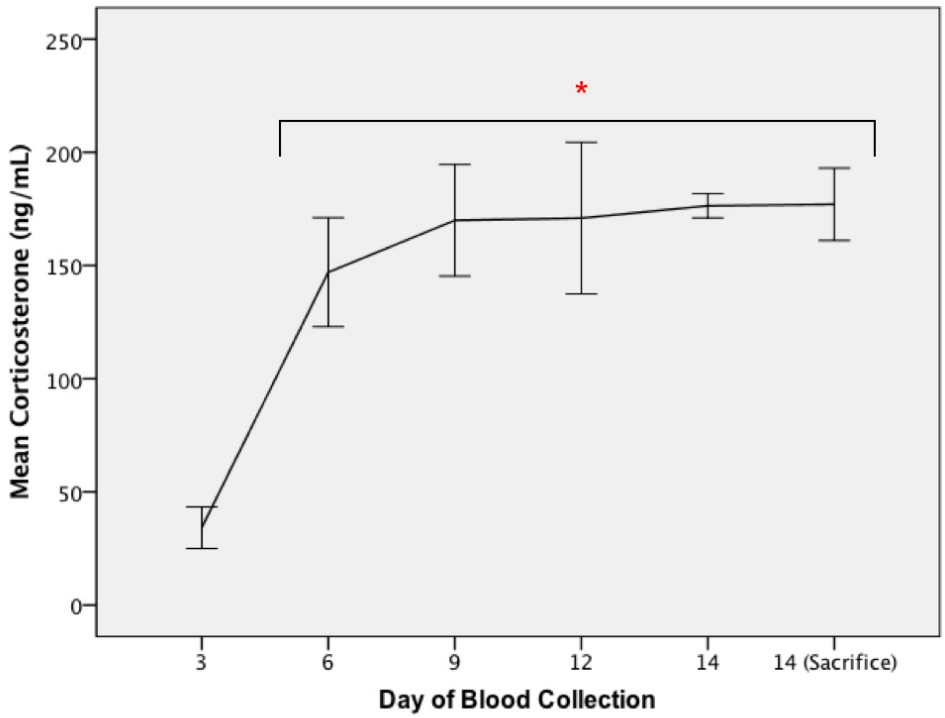

Figure 15. Variations in corticosterone levels during habituation in the first experimental series.

Mice (n = 7) were exposed to the experimenter during two handling sessions (days 1 & 2) and head-restrained on the wheel during seven habituation sessions (days 6-12) of increasing duration (10 – 40 minutes). Five blood samples were collected from the facial vein of each mouse (days 3, 6, 9, 12 and 14), in order to assess the variations in corticosterone levels throughout the habituation protocol. Trunk blood was also collected following sacrifice (day 14). Significance relative to the baseline value (day 3) is indicated by *.

Experimental Series 2

Experimental Design

For the second and third experimental series, we chose to follow a **between-subject design**, where mice were randomized to different habituation groups, and blood was collected only once per mouse (from the mouse trunk, following decapitation). This allowed to prevent potential increases in stress levels induced by repeated blood collection from the conscious mice.

In the second experimental series (**Figure 16**), mice (n = 12) were segregated into the following six groups. (1) Mice in the **Control** group were not exposed to any manipulation by the experimenter prior to sacrifice and hence provided baseline levels of corticosterone. Mice in all other groups were all implanted with a head bar (day 1), gently handled by the experimenter (~10 minutes on days 2 & 3) and restrained on the wheel for 30 minutes prior to sacrifice (day 9). (2) The **Non-Habituated** group was never exposed to the wheel prior to day 9; hence, we expected this group to display the highest stress levels as they were neither familiarized with the wheel, nor habituated to head restraint. In contrast, the remaining groups were habituated to the wheel for 10, 20, 30 and 40 minutes, on days 5-8, respectively. (3) The **Habituated** group was immediately sacrificed following habituation, whereas (4) the **Transferred** group was moved from the animal facility to the surgery room prior to sacrifice (day 9), in order to examine whether changing the environment of the mice increased their corticosterone levels significantly. Last, whilst the last two groups both underwent thinning of the cortex and LDF (day 9), (5) the **Conscious** group was awake during bone thinning, whereas (6) the **Anesthetized** group was administered with isoflurane beforehand. The latter two groups allowed to determine if the thinning procedure was a significant source of stress.

The purpose of this experimental series was to enable us to adjust specific components of the habituation protocol (handling, transfer to the surgery room, thinning with or without anesthesia, and optical imaging), in order to minimize the stress associated with each procedure. Further, by comparing **Non-Habituated** group with the groups which underwent acclimation to head restraint (the **Habituated**, **Transferred**, **Conscious** and **Anesthetized** groups), we would be able to conclude whether the habituation protocol was successful in reducing stress levels during immobilization on the wheel.

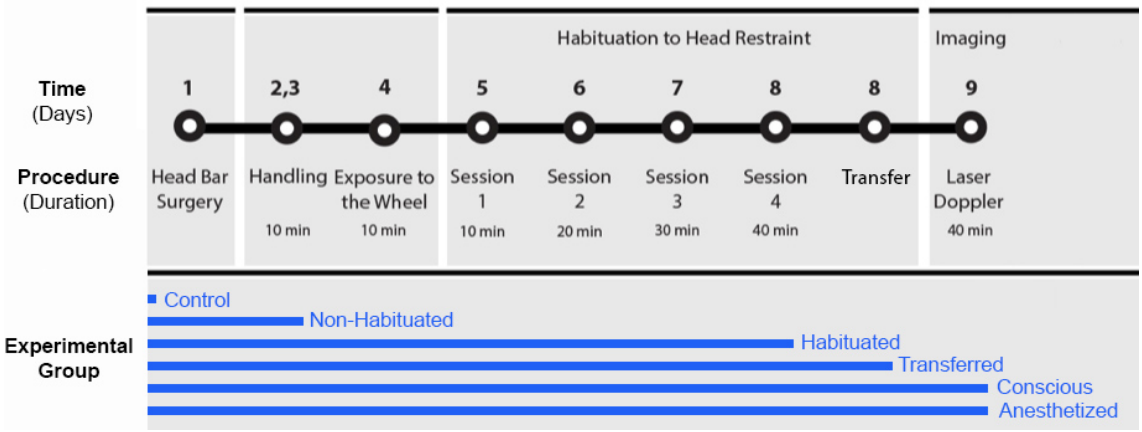

Figure 16. Protocol summary for habituation in the second experimental series.

Mice (n = 12) were segregated into six groups of equal size. The blue horizontal bars indicate the procedures undergone by each experimental group.

Findings

Compared with the Control group, corticosterone levels were increased by ~16-17 times in the Non-Habituated, Habituated and Transferred groups, and by ~10 times in the Conscious and Anesthetized groups (**Figure 17**); however, these differences were not significant ($F(5,6) = 1.43$, $p = 0.334$). The probability value was increased ($F(2,9) = 3.41$, $p = 0.079$) in a subsequent analysis where the mice that were habituated to the wheel (in the Habituated, Transferred, Conscious and Anesthetized groups) were combined into in a single group (n = 8), and post-hoc analyses

revealed a trend for increased corticosterone in these habituated mice relative to the Control group ($p = 0.085$). Notably, the corticosterone levels were highly variable in the Non-Habituated group (standard deviation: ±74.77 ng/mL), highlighting the need for larger experimental groups.

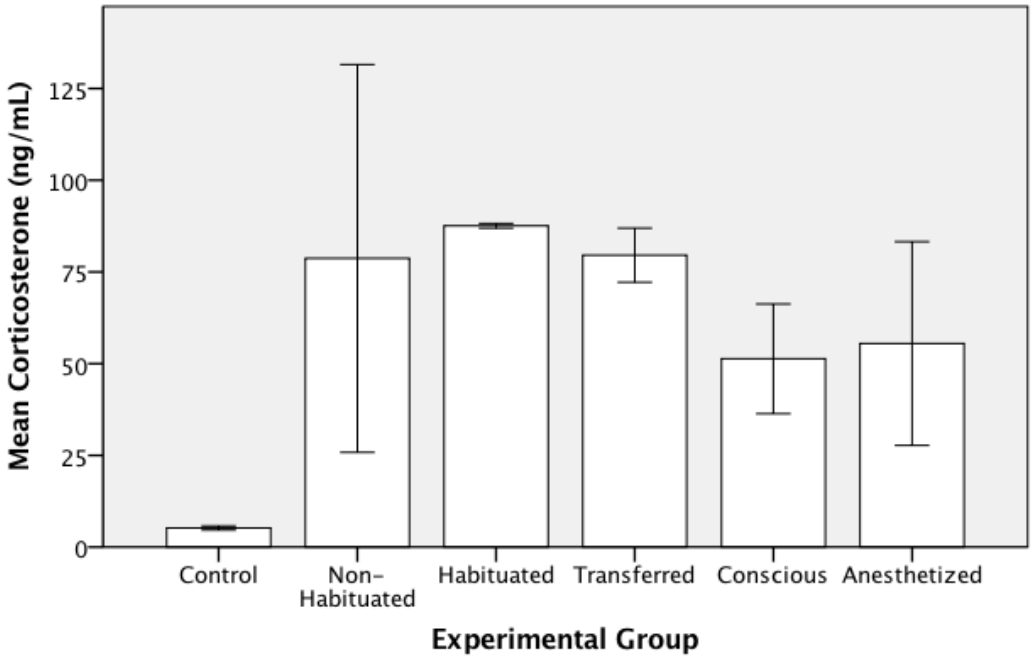

Figure 17. Differences in corticosterone levels between groups in the second experimental series.

Mice (n = 12) were segregated into six groups of equal size. (1) The Control group was never manipulated, whereas the (2) Non-Habituated group was handled prior to sacrifice. The remaining groups underwent 4 habituation sessions of increasing durations (10-40 minutes). (3) The Transferred group was moved to surgery room but did not undergo LDF. The Conscious and Anesthetized groups were both imaged with LDF; however, the (5) Anesthetized group was administered with isoflurane prior to bone thinning, whereas the (6) Conscious group was not. All mice (except Control) were head-restrained for 30 minutes immediately prior to sacrifice and blood collection.

Experimental Series *3*

Experimental Design

For the last experimental series, we sought to reduce the number of experimental conditions based on the obtained results. We attributed mice (n = 10) to three different groups, which were all transferred to the surgery room prior to sacrifice (day 16) (**Figure 18**). The **Control** group (n = 4) was not manipulated by the experimenter prior to sacrifice. The two remaining groups were both implanted with the head bar (day 1) and subjected to LDF (day 16); however, the **Non-Habituated** group (n = 3) was neither handled nor habituated to head restraint. In contrast, the **Habituated** group (n = 3) was handled by the experimenter (10 minutes, days 2 & 3), exposed to the wheel (10 minutes, day 4) and habituated to head restraint (15 minutes, days 5-15). This series was aimed at determining whether repeated exposure to head restraint was successful at reducing stress, independent of the length of the habituation sessions.

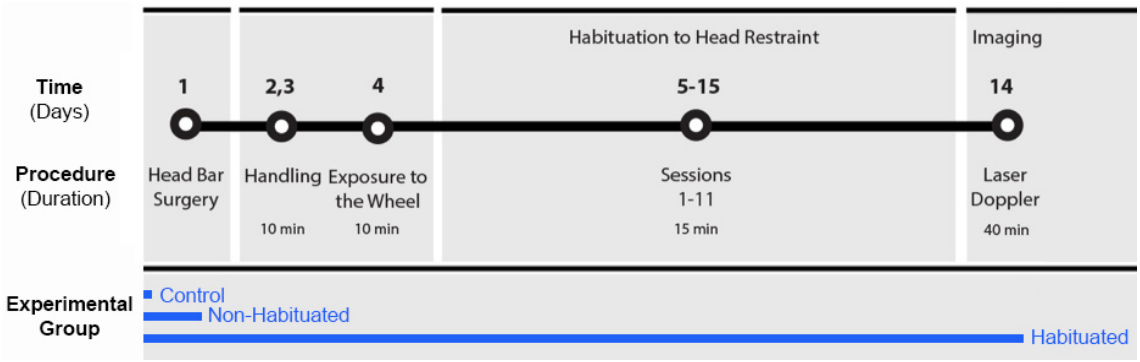

Figure 18. Protocol summary for habituation in the third experimental series.

Mice (n = 10) were segregated into three different groups. The blue horizontal bars indicate the procedures undergone by each experimental group.

Findings

Corticosterone levels were increased respectively by 18 and 20 times in the Habituated and Non-

Habituated groups, relative to control mice (**7.38** ± 3.45), with a strong trend towards significance (F (2, 7) = 4.45, p = 0.057); however, there was no significant difference between the Habituated and Non-Habituated groups. Moreover, we noted a large variance in the Habituated group (standard deviation: ±119.47 ng/ml) (**Figure 19**).

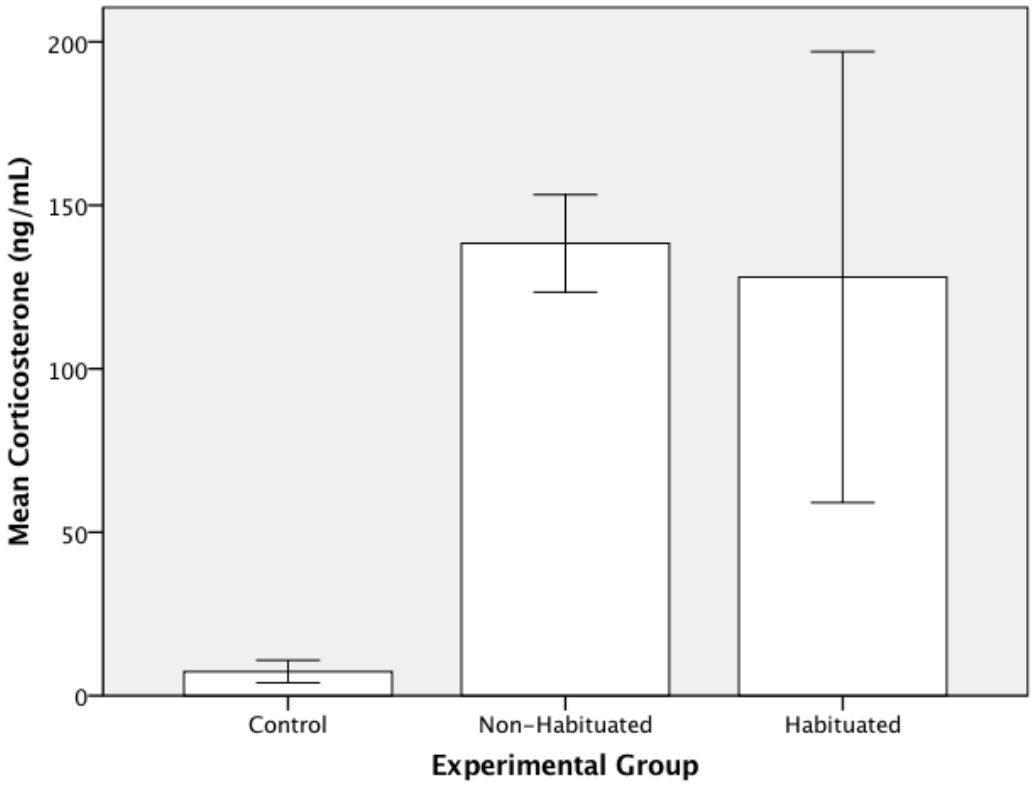

Figure 19. Differences in corticosterone levels between groups in the third experimental series.

Mice (n = 10) were segregated into 3 groups. (1) The Control group (n = 4) was never manipulated. (2) The Habituated group (n = 3) was handled, exposed to the wheel and habituated to head-restraint, whereas the Non-Habituated group (n = 3) was not.

Further Analyses

In a subsequent analysis, we combined similar experimental conditions from the three aforementioned series, in order to assess differences in corticosterone levels between mice that were never manipulated (**Control** group, n = 6), mice that were handled gently but never restrained (**Handled** group, n = 6), mice that were habituated prior to restraint (**Habituated** group, n = 11), and mice that were not habituated prior to restraint (**Non-Habituated** group, n = 5). The analysis was performed by one-way ANOVA and revealed significant differences between the groups ($F(3,24) = 6.270$, $p = 0.003$).

Using Tukey's multiple comparisons test, we found plasma corticosterone to be significantly increased in the Habituated group (**84.72** ± 2.23) relative to the Control group (**6.65** ± 2.23) ($p = 0.017$), and in the Non-Habituated group (**114.50** ± 23.66) relative to the Control group ($p = 0.05$) and Handling group (**34.22** ± 9.21) ($p = 0.047$) (**Figure 20**).

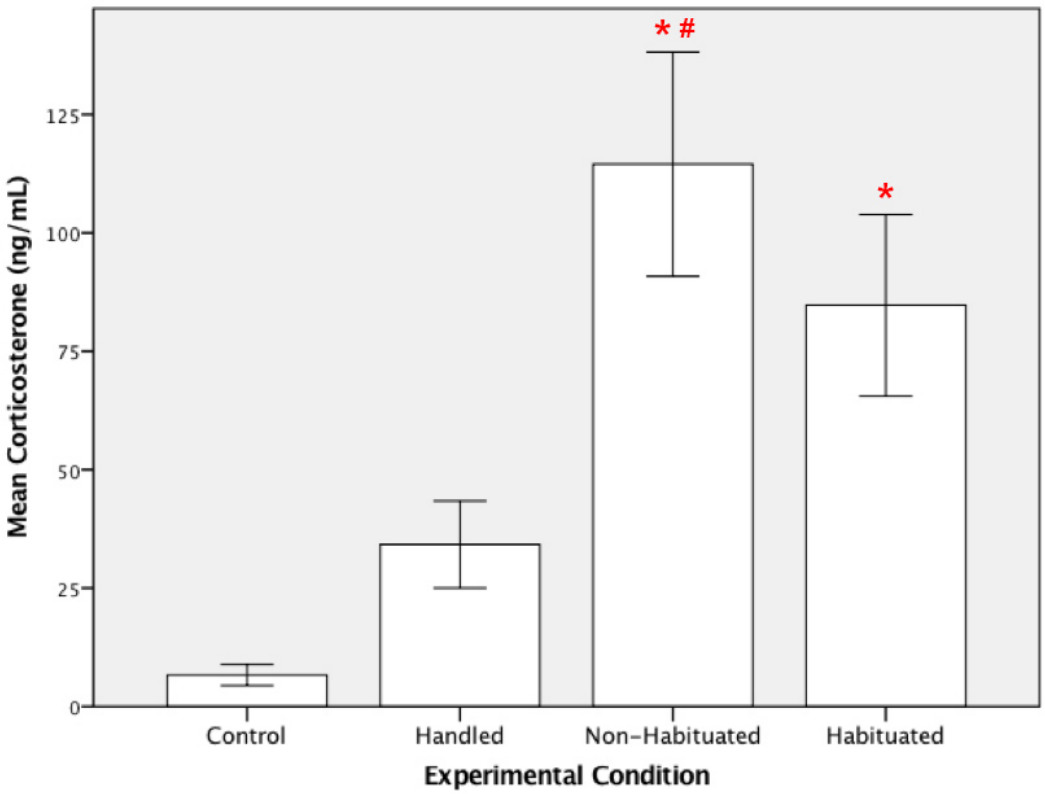

Figure 20. Differences in corticosterone levels between different experimental conditions.

Control mice (n = 6) were never manipulated, whereas Handled mice (n = 6) were handled by the experimenter prior to sacrifice. Habituated (n = 11) and Non-Habituated mice (n = 5) were both restrained on the wheel for LDF, however only the Habituated mice underwent habituation prior to restraint. Significance relative to the Control and to the Handled groups is indicated by * and #, respectively.

Discussion

Most optical imaging studies of the cerebral vasculature in rodents have been performed under general anesthesia, in order to prevent motion-induced artifacts and minimize stress induction during image acquisition. However, anesthetics have been demonstrated time and again to exert profound effects on cerebral hemodynamics, thereby altering neuronal responsiveness to sensory stimulation and hindering the study of NVC in health and disease [66, 75, 280, 281] (see **Figures 11 – 13**). Consequently, many research groups have turned to the use of awake imaging, where full [271, 273, 282] or partial physical restraint [132, 140, 191, 270, 274, 276, 283-291] of the conscious animal is used as a substitute for anesthesia, in order to keep the animal's head still whilst the signal is being acquired. Nevertheless, physical restraint may increase the levels of stress in rodents, which could, similarly to anesthetics, interfere with CBF and resting cerebral metabolism (see **Section 3**).

In the present study, our **general aim** was to develop an awake imaging model which would enable the study of NVC in the conscious, head-restrained mouse, whilst overcoming the effects of anesthesia and stress on the cerebral vasculature. For this purpose, we have built a new head-restraint apparatus for imaging of the cerebral vasculature in awake behaving mice. In order to minimize struggling and motion-induced artifacts during image acquisition, we have tested several training regimens, which gradually accustom mice to the restraint apparatus. Furthermore, we have set out to provide, for the first time, a quantitative measure of the evolution of stress, as a means to validate the effectiveness of our habituation protocol in decreasing restraint-induced stress in mice prior to awake optical imaging.

1. Development of a head-restraint apparatus for optical imaging in awake behaving mice (objective 1)

Awake imaging has constituted a major advancement for the study of the cerebrovascular system, allowing to sidestep the physiological confounds associated with general anesthesia. To date, most awake imaging studies in rodents have been performed using an air-lifted spherical treadmill [132, 140, 191, 274, 276, 283-290], pioneered by Dombeck's group ten years ago [270]. Using this setup, the animal is head-fixed by the means of a metal head plate and allowed to rest or walk on a Styrofoam ball (~8 inch) at its will. The ball is levitated under the microscope using pressurized air and hence can rotate with the animal's movement. Moreover, the movement of the Styrofoam ball can be recorded using optical sensors, thereby enabling to study the effect of locomotion on neuronal and cerebrovascular function.

Nevertheless, this treadmill is associated with several practical limitations for our purposes. First, the large size of the setup equipment would preclude its use with certain experimental setups. Furthermore, in order to achieve levitation, the spherical treadmill requires a constant flow of pressurized air, which not only is associated with incessant noise that can be stressful for the mouse, but also, may become problematic during experiments which involve long-lasting imaging sessions. This also holds true other awake imaging systems such as the air-lifted homecage developed by Kislin's group, which necessitates a significate amount of pressurized air in order to achieve levitation [274]. Lastly, the round, smooth surface of the Styrofoam ball provides an unnatural running platform for laboratory mice relative to the cage floor, and running is at first erratic and inconsistent, as the animals adapt to moving on the ball [276].

Hence, in accordance with our **first objective**, we have developed a new setup for head-

restraint in the awake behaving mouse, which is more compact and suitable for use with most optical imaging platforms used to study NVC, including LDF, LSCI, OIIS and TPLSM. This device is inexpensive, easy to assemble and de-assemble, and can be swiftly adjusted in order to allow the mice to assume a comfortable posture. All parts were purchased from the same vendor (ThorLabs, NY, USA), except the wheel was designed in Autodesk software and built with a 3D printer. This additive manufacturing technique enables easy design replication by other experimenters and permits size modifications, so that our head-restraint device can be built for other small animals or adjusted per experimental requirements. The head post allows for sturdy immobilization of the head, which is essential to minimize motion-induced signal artifacts, and can be raised according to the animal's height. As for the wheel, it was designed with a solid, ridged running surface for better grip, and could be moved laterally, in order to allow for the natural movement of the animal. In conjunction with the aforementioned device, we have developed a habituation protocol, in order to help the mice to adapt to head-restraint and minimize the stress experienced during the imaging sessions.

2. Habituation to head-restraint (objective 2)

Since most optical imaging modalities are highly sensitive to motion (see **Section 4**), head-restraint of the animal during image acquisition is inevitable. However, head-restraint is known to induce significant stress in mice that are naïve to the condition [292], which in turn, can affect cerebral hemodynamics (see **Section 3**). Hence, it is essential that measures are taken to reduce stress in the restrained animals, especially in studies which tackle the regulation of the CBF.

Indeed, whilst some groups have proceeded to image in the naïve mouse [140, 283, 293], rodents were usually trained to tolerate head-restraint, during a habituation period lasting

anywhere between a single day [271] and several weeks [272, 282] (see **Table 3**). In the more conservative protocols, mice were first handled by the experimenter and were allowed to run freely on the device without head-restraint for at least one session. Subsequently, daily head-restraint sessions of increasing duration (typically up to 45 minutes) were performed in order to minimize the stress experienced by the mice during the following imaging sessions. Based on qualitative observations, several groups have found that between the second and the fourth habituation session, mice learned to walk or run on the device, and initiated grooming behavior when stationary [191, 271, 274]. Hence, these data suggest that a 4-day habituation protocol may be sufficient to acclimate the mice to head-restraint.

In the present study, we have designed three separate habituation protocols, ranging from 4 to 11 sessions of habituation to head-restraint, based on the aforementioned data and our results. For all protocols, mice were handled on the two first days by placing them into the experimenter's hands until they initiated grooming behavior (~5-10 minutes), as previously reported [191, 270, 272-274, 282]. Handling ensured that the mice became familiar with the experimenter's voice, smell and touch throughout the habituation protocol, and were accustomed to being picked up by this person [292]. Indeed, we noted that the mice were noticeably calmer by the second handling session, as they were less agitated, explored the hands of the experimenter and initiated grooming more rapidly, relative to the first session. The mice continued to be handled briefly (~5 min) prior to each manipulation session throughout the experiment. During the third session, mice were gently placed on the wheel and allowed to explore it for 10 minutes without restraint. We found that all mice adapted to running on the wheel quickly, with some of them demonstrating exploratory and grooming behavior when

stationary.

In subsequent sessions, mice were exposed to either gradually incremented head-restraint sessions (from 10 to 40 minutes; experimental series 1 and 2), or for repeated periods of the same duration (15 minutes; experimental series 3). Whilst during the first head-restraint session, some of the mice struggled against the head-post, emitted vocalizations and displayed decreased locomotion and increased urination, we found that using either type of protocol, these behaviors were noticeably reduced within the following two sessions. Hence, based on these qualitative observations, we have successfully met our **second objective** by designing a three-step training approach, which allowed mice to adapt to running on the wheel and minimized overt signs of stress (struggling, vocalizations and urination), in preparation for imaging of the CBF. Nevertheless, we sought to validate our observations quantitatively, by using plasma corticosterone as a surrogate marker of stress.

Table 3. List of protocols designed to habituate mice to head-restraint in preparation for optical imaging.

References	Restraint Device	Habituation Protocol	Comments
[283]	Spherical treadmill	No training	Mice were head-fixed under anesthesia with isoflurane, and showed no signs of struggling against head-restraint
[140]		No training	Repeated experiments over 7 days revealed a stable CBF response to whisker stimulation.
[276]		- No handling - Session 1: **head-restraint** (30min) - Session 2: **head-restraint** (45 min) Head-restraint sessions included 15 min of uninterrupted running, followed by whisker stimulation.	During head-restraint, mice showed several observable behaviors including being quiet, running or grooming. Adding more than 2 head-restraint sessions led to little behavioral improvement.
[294]		1-3 daily head-restraint sessions (15-30 min).	-
[270]		Session 1: handling (10min) + free running (10min). Session 2: free running (10-15min). Session 3: surgery + **head-restraint** (15-20min).	During the third session, mice learned to balance and started to walk or run within 5-10 minutes.
[293]		Not all mice were habituated to head-restraint: - Session 1 & 2: free running (for all mice, n = 10). - Sessions 3-5: **head-restraint** (for only 3/10 mice).	For the 7 mice that weren't habituated to head-restraint, it took ~10-15 min to learn to balance and start walking or running on the ball. The 3 mice that were head-restrained started to walk and run immediately.
[288]		3-4 Days: mice were habituated to tolerate 1-2 hours of **head-restraint**	-
[290]		5 consecutive days of habituation to **head-restraint**	-
[60]		3-7 days: **head-restraint**	-
[191]		Session 1: handling + free running (10 min) Sessions 2-5: **head-restraint** (30 min; i.e. 10 min with lights on + 20 min with lights off) Session 6 & 7: **head-restraint** & whisker stimulation (30 min)	After 2-3 sessions of head-restraint, mice learned to move freely on the ball and initiated grooming behavior when stationary.
[274]	Air-lifted platform	- Handling - 8-12 **head-restraint** sessions (2 hrs), twice per day.	Initial weight loss and suppression in locomotor activity induced by head-restraint were reversed by day 4 of training.
[272]	Head-post	- Minimum 2 weeks: handling & **head-restraint** - Minimum 1 week: 2 **head-restraint** sessions per day; gradual increase duration from few seconds to 45 minutes.	During the first 2 weeks, the mice accepted head-fixation without any sign of stress.
[271]	Semi-circular plastic tube	2 training sessions on the same day: Session 1: **head-restraint** (15min) at 8am. Session 2: **head-restraint** (30 min) at 4pm.	Mice habituated to restraint within 2–3 sessions, judging from a marked decrease in walking & running.
[282]		- 3-14 days: handling (> 5 min, or until grooming). - 1-2 weeks: **restraint** (gradual increase from 5 min to > 1 h).	-
[273]	Foam-restraining device	Mice were handled every day after weaning and were restrained (1-5 min) for 1 week.	Exposure to handling and restraint enabled long recording sessions (up to 4-5 hours) with reduced motion and stress of the mouse.

3. Quantitative evaluation of stress (objective 3)

Following the induction of stress in mice, activation of the hypothalamic–pituitary–adrenal axis initiates the secretion of corticotropin-releasing hormone and vasopressin from the parvocellular neurons in the paraventricular nucleus of the hypothalamus. Following release, these neuropeptides bind to corticotrophs in the anterior pituitary gland, leading to the synthesis of adrenocorticotropic hormone which is then secreted into the general circulation. Binding of the adrenocorticotropic hormone in the adrenal cortex induces the downstream release of glucocorticoids, including cortisol and corticosterone [295, 296].

Corticosterone is the main hormone involved in the regulation of stress in rodents, and has been demonstrated to impair NVC in rats, possibly by acting on glucocorticoid receptors in VSMCs [3]. Moreover, corticosterone has been shown to constitute a better adaptation-related marker during situations of chronic stress, relative to cortisol [279]. Based on these data, we have chosen to measure the variations of corticosterone levels in mice throughout habituation to head-restraint. Notably, whilst corticosterone levels have been previously measured in awake mice in non-invasive medical imaging studies (**Table 4**), ***the current study constitutes the first attempt at providing a quantitative measure of stress in an awake, optical imaging experiment***.

In our first experimental series, we noted a 10-fold increase in corticosterone subsequent to head-restraint, which was maintained across 7 habituation sessions ($p < 0.05$). We hypothesized that the repeated puncturing of the facial vein for blood collection may have conditioned the mice to associate head-restraint on the wheel with pain, thus preventing corticosterone from reverting to baseline levels. Consequently, in our second and third series,

blood was only collected from the trunk following sacrifice, which is the predominant method amongst previous studies [279, 297-299] (**Table 4**). Nevertheless, we did not observe a significant effect of habituation sessions on plasma corticosterone, possibly due to the large variance in corticosterone levels in the Non-Habituated (**experimental series 2**) and Habituated groups (**experimental series 3**). Notably, such individual variation amongst awake mice has been noted by Baba and colleagues, whereby corticosterone levels were increased between 1.8 and 8.76 times following a one-hour placement in a single-photon emission computed tomography (SPECT) scanning burrow [299]. In addition, mice which were restrained using our device had corticosterone levels (85 – 115 ng/ml) comparable to those reported by Mizuma's group following restraint in a PET scanner (~150 ng/ml) [300], indicating that the stress experienced in our conditions was similar to, if not milder than that in medical imaging studies.

That said, in two medical imaging studies, corticosterone levels were reduced to at least twice the baseline levels as the rodents habituated to the imaging conditions [300, 301], which was not observed under our experimental conditions. Nevertheless, we noted that mice in the Conscious and Anesthetized groups (**experimental series 2**) exhibited corticosterone levels in the range of 27 – 84 ng/mL, which is at least twice as low as the levels observed on the first day of restraint in all published studies. In particular, these mice (n = 4) have been subjected to LDF imaging in our second experimental series, and as a result were left for thirty minutes in a dark, silent environment (in the surgery room) for the CBF to stabilize (see **Methods, Section 5**), whilst the other groups were not.

Hence, increasing the group size in order to counter the large individual variability in glucocorticoid levels, and modifying the restraint environment may yield a significant reduction

in corticosterone subsequent to habituation sessions. In addition, it has been suggested that immobilizing rodents whilst leaving their body exposed in an open space may be perceived by the animals as a threatening position, thereby generating anxiety [292]. Accordingly, placing the rodent in an enclosed space such as a medical imaging scanner, or covering the body with a dark, loose-fitting material during optical imaging sessions may further help to reduce corticosterone levels.

Lastly, whilst we have included brief handling in our habituation protocol at the beginning of each restraint session, based on our behavioral observations and previous reports (**Table 3**), we found corticosterone levels to be increased by 27.68 ng/mL in Handled mice relative to Control mice. This increase was not significant as there was a high variability in the Handled group (standard deviation: ±22.56), indicating that mice may each respond to experimental manipulation differently. Interestingly, Tran's group reported to have eliminated experimental handling from their habituation protocol, as they found no improvement in stress behaviors, relative to mice that were not initially handled. In fact, quite on the contrary, gentle handling for 6 days has been reported to cause a mild increase in corticosterone levels in mice (from 45 to 60 ng/mL), and is even used in some studies to induce total sleep deprivation in these animals [298]. Taken together, these data indicate that repeated handling may induce a gradual sensitization of the hypothalamic–pituitary–adrenal axis, thereby leading to a sustained elevation in plasma corticosterone and resulting in learned helplessness.

Table 4. Variations in corticosterone levels induced by different types of manipulations.

References	Type of Rodent	Type of Manipulation	Protocol for Acclimation & Blood Collection	Variations in Corticosterone levels (ng/ml)	Comments
[298]	Mice	Gentle Handling	2 groups of mice (n = 8 each) were gently handled or left undisturbed for 6 days. Trunk blood was collected at 12:00 on the next day.	There was a delayed increase in corticosterone on day 6 of handling (60 ng/ml), relative to undisturbed animals (45 ng/ml) ($p < 0.05$).	The effects of repeated brief handling on murine physiology persists or even strengthens within 6 days, indicating poor adaptation.
[279]		Repeated restraint	Mice (n = 6) were restrained daily for 8 h in individual micro-cages. Trunk blood was collected immediately after the end of the stress period.	Corticosterone rose from ~0 ng/ml (day 0) to ~900 ng/ml (day 1), before decreasing to ~300 ng/ml (day 8) ($p < 0.05$).	In contrast with repeated restraint, mice did not habituate to unpredictable stress, as the increase in corticosterone (900 ng/ml) was maintained for 9 days.
[300]		Restraint in a PET scanner	Blood was collected from left ventricle of anesthetized mice (n = 5). Corticosterone was measured 1 h after head-fixation, on days 1, 3, 13 and 20 of acclimation.	- 3.75-fold increase (150 ng/ml) from baseline levels (40 ng/ml) on the first day after head-bar surgery - Decreased to twice the levels of baseline, 30 days after surgery	In spite of the lengthy acclimation period, corticosterone levels didn't revert to the baseline levels found in intact mice housed in their home-cage.
[299]		Awake-SPECT scan (no restraint)	No surgery or training. Blood was withdrawn from the tail vein of mice (n = 3) immediately after the mock scan.	The scan induced between an 1.8 and 8.76-fold increase, after 1 h placement in the scanning burrow.	This increase was highly variable, and in 2 of the 3 mice, was on the order of that observed in mice exposed to rat odors (1.86-2.6-fold) [302].
[297]	Rats	Restraint in Plexiglas	Rats (n = 6) were restrained in a Plexiglas restraint device. Trunk blood was collected following decapitation.	Corticosterone levels increased from ~200 to ~470 ng/ml after 15 min of restraint.	This increase was similar to that induced by a 20 min footshock, 1 h of rotatory stress or 3 days of 1 h-cold exposure.
[301]		Restraint in fMRI scanner	Rats (n=8) were anesthetized and restrained in a mock fMRI scanner with scanner noise during daily 90 min acclimation sessions, for 8 days. Blood was collected immediately after restraint via eye bleed.	Corticosterone increased initially (first 3 days), then decreased dramatically (days 5 & 8) from ~240 to baseline (~60 ng/ml), $p < 0.05$.	- Respiration and heart rate decreased significantly on day 3 of acclimation. - Head motion and noise were also decreased. - Regional CBF was altered with acclimation.
[303]		Attachment of a miniature PET scanner (no restraint)	Corticosterone was measured in rats (n = 2). Jugular vein catheters were implanted for blood sampling. Sampling took place before and 10 min, 1 h, 2 h and 3 h after attachment of a miniature PET scanner.	After 10 min, corticosterone increased by 4-fold (~800 ng/ml). After 3h, corticosterone nearly normalized in 1 rat, and decreased to about twice the baseline levels in the other rat (~200 ng/ml).	-
[251]		Restraint in plastic bag	Rats (n = 10) were immobilized 2 h per day, for 3 weeks. Cardiac blood was collected under anesthesia, immediately following restraint.	Plasma corticosterone was significantly elevated (n = 10, 96.19), compared with the control group (n = 10, 256.27) ($p = 0.002$).	In the forced swim test, rats showed decreased swimming and increased immobility, indicative of behavioral despair.

Conclusion and Future Directions

In conclusion, we have developed a new head-restraint device for optical imaging in the awake behaving animal. This device is compatible with several imaging modalities, including LDF, LSCI, OIIS and TPLSM. In addition, we have developed a habituation protocol which, although it noticeably decreased overt signs of stress in mice, did not have a significant effect on corticosterone levels. This was possibly due to animal handling or consistent discomfort elicited by the device, which has led to poor adaptability of mice to head-restraint.

For prospective studies, we recommend eliminating animal handling from the habituation protocol, which we expect would reduce the variability in corticosterone levels within different experimental conditions, as the reaction of each animal to the experimenter's touch, voice and scent can be different. Furthermore, it would be important to use additional physiological (heart rate and breathing rate) and behavioral (open field test or forced swim test) measures of stress. This would allow to verify whether the behavioral changes observed in the mice following habituation were induced by a reduction in stress levels or by learned helplessness. Indeed, Lee and colleagues found that restraining rats in a plastic bag (2 h per day, for 3 weeks) led to substantial increase in corticosterone (from 96.19 to 256.27 ng/mL, $p = 0.002$), in addition to decreasing swimming and increasing immobility in the forced swim test, which is indicative of behavioral despair [251]. In contrast, habituation to restraint in a mock fMRI scanner (90 min per day, for 8 days) induced a significant decrease in the respiratory and heart rate on day 5 ($p < 0.05$), and reduced corticosterone levels from ~240 ng/mL on day 1 back to baseline levels on day 8 (~60 ng/mL, $p < 0.05$), suggesting that the rats had successfully adapted to the scanning

conditions [301]. Accordingly, in addition to measuring serum corticosterone with ELISA, we sought to set up an open field chamber (OFC) to be used in prospective studies as a complementary method for determining stress levels in mice. The OFC is one of the most commonly used platforms to evaluate anxiety-related behaviors in mice [304]. We will use a 42 x 42 x 29 cm quadratic chamber with Plexiglas floor and walls, which was custom-built by Lesage laboratory at Polytechnique Montreal (see **Figure 21**). Thirty-three infrared photo-emitters and photo-receivers are interspaced at equal intervals along the perimeter of the OFC walls. These emitters and receptors create an x-y grid of invisible infrared laser beams. At the beginning of each trial, a mouse is placed in the middle of the chamber for a 10-minute test period. The mouse's movement within the chamber breaks the laser beams, thus providing information about the mouse's basal locomotor activity (centimeters), time spent in the periphery (known as *thigmotaxis*), time spent in the central zone of the chamber, movement time and rest time (seconds). Additional behavioral measures such as defecation count and grooming behavior can be assessed visually using a scoring sheet. Decreased locomotor activity, time spent in the center, movement time and grooming behavior, and increased thigmotaxis, rest time and defecation would reflect a rise in the mouse's stress levels [304].

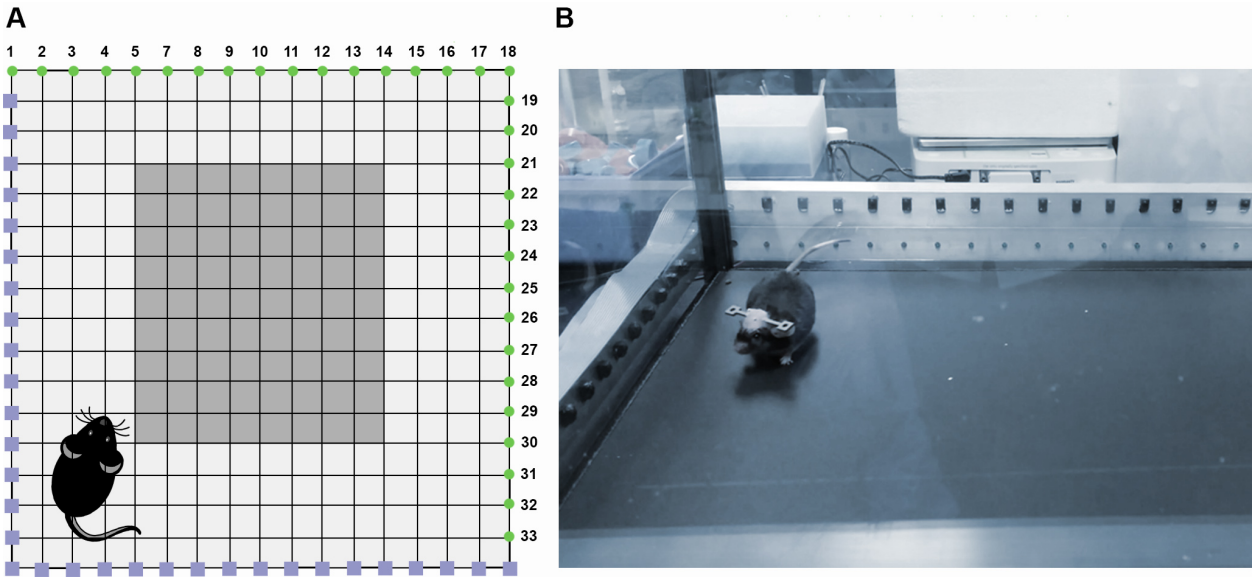

Figure 21. Custom-made open field chamber.

(A) Diagram of the open field chamber, showing the laser grid formed by the light emitters (green) and receivers (blue). The disruption of the laser beams provides information about the mouse's location within the center (dark grey) or periphery (light grey) of the chamber, as well as the total distance travelled (cm), and the time spent resting and moving (sec). (B) Photo of the open field chamber built by Lesage laboratory.

Moreover, for restraint devices to which animals seem to adapt poorly, it would be interesting to use a graded exposure technique, whereby gradually increased restraint sessions are paired with a liquid reward. This method is based on human behavioral modification which has been met with success amongst patients suffering from phobias, and was shown to be effective in conditioning studies in rodents [305]. Indeed, two groups have reported using water scheduling [294] or a sweet reward [191] in order to help head-restraint mice adapt to running on a Styrofoam ball. Whilst another group has anesthetized rodents prior to head-fixation in order to reduce stress [303], anesthesia is likely to have lasting effects on cerebrovascular dynamics (see **Section 3**) and therefore is best avoided.

Notably, King and colleagues found regional CBF to be altered subsequent to acclimation to restraint in an fMRI scanner [301], indicating that restraint-induced stress does indeed affect

the CBF. As such, it would be essential to also evaluate how the hemodynamic response is affected by head-restraint and by subsequent acclimation to our device. Ultimately, this would allow us to determine if the device we have designed is valid for investigating the neurovascular response, or whether it needs to be altered in order to improve the mouse's adaption and prevent the effects of stress on the cerebral vasculature.

References

1. Iadecola, C., *Neurovascular regulation in the normal brain and in Alzheimer's disease.* Nat Rev Neurosci, 2004. **5**(5): p. 347-60.
2. Cauli, B. and E. Hamel, *Revisiting the role of neurons in neurovascular coupling.* Front Neuroenergetics, 2010. **2**: p. 9.
3. Longden, T.A., et al., *Stress-induced glucocorticoid signaling remodels neurovascular coupling through impairment of cerebrovascular inwardly rectifying K+ channel function.* Proc Natl Acad Sci U S A, 2014. **111**(20): p. 7462-7.
4. Gao, Y.R. and P.J. Drew, *Effects of Voluntary Locomotion and Calcitonin Gene-Related Peptide on the Dynamics of Single Dural Vessels in Awake Mice.* J Neurosci, 2016. **36**(8): p. 2503-16.
5. Cipolla, M.J. and M.J. Cipolla, *The cerebral circulation*. Colloquium series on integrated systems physiology, from molecule to function 2. 2010, San Rafael, CA: Morgan & Claypool. 1 electronic text (x, 59a : ill.) : digital file.
6. Schünke, M., E. Schulte, and U. Schumacher, *Thieme atlas of anatomy*. 2010, Stuttgart: Thieme. xiii, 412 : col. ill. ; 32 cm.
7. Schünke, M., E. Schulte, and U. Schumacher, *General anatomy and musculoskeletal system : latin nomenclature*. Thieme Atlas of Anatomy. 2005, Stuttgart: Thieme. 541.
8. Liebeskind, D.S., *Collateral circulation.* Stroke, 2003. **34**(9): p. 2279-84.
9. Hossmann, K.A., *Pathophysiology and therapy of experimental stroke.* Cell Mol Neurobiol, 2006. **26**(7-8): p. 1057-83.
10. Golgi, C., *Sulla fina anatomia degli organi centrali del sistema nervoso. Studi, etc*. 1886, Milano. 214 ; 8º.
11. Peters, A., S.L. Palay, and H.d. Webster, *The fine structure of the nervous system : neurons and their supporting cells*. 1991, New York ; Oxford: Oxford University Press. xviii, 494 : ill. ; 28 cm.
12. Edvinsson, L. and D.N. Krause, *Cerebral blood flow and metabolism*. 2002, Philadelphia, Pa: Lippincott Williams & Wilkins. xvii, 521 , 8 of plates : ill. ; 29 cm.
13. Hamel, E., *Perivascular nerves and the regulation of cerebrovascular tone.* J Appl Physiol (1985), 2006. **100**(3): p. 1059-64.
14. Cohen, Z., G. Molinatti, and E. Hamel, *Astroglial and vascular interactions of noradrenaline terminals in the rat cerebral cortex.* J Cereb Blood Flow Metab, 1997. **17**(8): p. 894-904.
15. Hossmann, K.A., *Viability thresholds and the penumbra of focal ischemia.* Ann Neurol, 1994. **36**(4): p. 557-65.
16. Panerai, R.B., *Assessment of cerebral pressure autoregulation in humans--a review of measurement methods.* Physiol Meas, 1998. **19**(3): p. 305-38.
17. Phillips, S.J. and J.P. Whisnant, *Hypertension and the brain. The National High Blood Pressure Education Program.* Arch Intern Med, 1992. **152**(5): p. 938-45.
18. Osol, G., et al., *Myogenic tone, reactivity, and forced dilatation: a three-phase model of in vitro arterial myogenic behavior.* Am J Physiol Heart Circ Physiol, 2002. **283**(6): p. H2260-7.
19. Cipolla, M.J. and G. Osol, *Vascular smooth muscle actin cytoskeleton in cerebral artery forced dilatation.* Stroke, 1998. **29**(6): p. 1223-8.

20. Bayliss, W.M., *On the local reactions of the arterial wall to changes of internal pressure.* J Physiol, 1902. **28**(3): p. 220-31.
21. Cipolla, M.J., et al., *SKCa and IKCa Channels, myogenic tone, and vasodilator responses in middle cerebral arteries and parenchymal arterioles: effect of ischemia and reperfusion.* Stroke, 2009. **40**(4): p. 1451-7.
22. Nilsson, T., et al., *Contractile 5-HT1B receptors in human cerebral arteries: pharmacological characterization and localization with immunocytochemistry.* Br J Pharmacol, 1999. **128**(6): p. 1133-40.
23. Busija, D.W. and D.D. Heistad, *Factors involved in the physiological regulation of the cerebral circulation.* Rev Physiol Biochem Pharmacol, 1984. **101**: p. 161-211.
24. Davis, M.J. and M.A. Hill, *Signaling mechanisms underlying the vascular myogenic response.* Physiol Rev, 1999. **79**(2): p. 387-423.
25. Semplicini, A. and L. Calo, *Administering antihypertensive drugs after acute ischemic stroke: timing is everything.* CMAJ, 2005. **172**(5): p. 625-6.
26. Gulbenkian, S., R. Uddman, and L. Edvinsson, *Neuronal messengers in the human cerebral circulation.* Peptides, 2001. **22**(6): p. 995-1007.
27. MacKenzie, E.T. and B. Scatton, *Cerebral circulatory and metabolic effects of perivascular neurotransmitters.* CRC Crit Rev Clin Neurobiol, 1987. **2**(4): p. 357-419.
28. Morita, Y., J.E. Hardebo, and E. Bouskela, *Influence of cerebrovascular sympathetic, parasympathetic, and sensory nerves on autoregulation and spontaneous vasomotion.* Acta Physiol Scand, 1995. **154**(2): p. 121-30.
29. Kontos, H.A., et al., *Responses of cerebral arteries and arterioles to acute hypotension and hypertension.* Am J Physiol, 1978. **234**(4): p. H371-83.
30. Sandrone, S., et al., *Weighing brain activity with the balance: Angelo Mosso's original manuscripts come to light.* Brain, 2014. **137**(Pt 2): p. 621-33.
31. Roy, C.S. and C.S. Sherrington, *On the Regulation of the Blood-supply of the Brain.* J Physiol, 1890. **11**(1-2): p. 85-158 17.
32. Attwell, D. and S.B. Laughlin, *An energy budget for signaling in the grey matter of the brain.* J Cereb Blood Flow Metab, 2001. **21**(10): p. 1133-45.
33. Hoffmeyer, H.W., et al., *Nonlinear neurovascular coupling in rat sensory cortex by activation of transcallosal fibers.* J Cereb Blood Flow Metab, 2007. **27**(3): p. 575-87.
34. Lee, J.H., et al., *Global and local fMRI signals driven by neurons defined optogenetically by type and wiring.* Nature, 2010. **465**(7299): p. 788-92.
35. Norup Nielsen, A. and M. Lauritzen, *Coupling and uncoupling of activity-dependent increases of neuronal activity and blood flow in rat somatosensory cortex.* J Physiol, 2001. **533**(Pt 3): p. 773-85.
36. Petzold, G.C., et al., *Coupling of neural activity to blood flow in olfactory glomeruli is mediated by astrocytic pathways.* Neuron, 2008. **58**(6): p. 897-910.
37. Sobey, C.G. and F.M. Faraci, *Effect of nitric oxide and potassium channel agonists and inhibitors on basilar artery diameter.* Am J Physiol, 1997. **272**(1 Pt 2): p. H256-62.
38. Faraci, F.M. and C.G. Sobey, *Role of soluble guanylate cyclase in dilator responses of the cerebral microcirculation.* Brain Res, 1999. **821**(2): p. 368-73.
39. Ma, J., et al., *Regional cerebral blood flow response to vibrissal stimulation in mice lacking type I NOS gene expression.* Am J Physiol, 1996. **270**(3 Pt 2): p. H1085-90.
40. Mathiisen, T.M., et al., *The perivascular astroglial sheath provides a complete covering of the brain microvessels: an electron microscopic 3D reconstruction.* Glia, 2010. **58**(9): p.

1094-103.
41. Bushong, E.A., et al., *Protoplasmic astrocytes in CA1 stratum radiatum occupy separate anatomical domains.* J Neurosci, 2002. **22**(1): p. 183-92.
42. Filosa, J.A., et al., *Local potassium signaling couples neuronal activity to vasodilation in the brain.* Nat Neurosci, 2006. **9**(11): p. 1397-1403.
43. Price, D.L., et al., *Distribution of rSlo Ca2+-activated K+ channels in rat astrocyte perivascular endfeet.* Brain Res, 2002. **956**(2): p. 183-93.
44. Higashimori, H., et al., *Role of epoxyeicosatrienoic acids as autocrine metabolites in glutamate-mediated K+ signaling in perivascular astrocytes.* Am J Physiol Cell Physiol, 2010. **299**(5): p. C1068-78.
45. Kuschinsky, W., et al., *Perivascular potassium and pH as determinants of local pial arterial diameter in cats. A microapplication study.* Circ Res, 1972. **31**(2): p. 240-7.
46. McCarron, J.G. and W. Halpern, *Potassium dilates rat cerebral arteries by two independent mechanisms.* Am J Physiol, 1990. **259**(3 Pt 2): p. H902-8.
47. Knot, H.J., P.A. Zimmermann, and M.T. Nelson, *Extracellular K(+)-induced hyperpolarizations and dilatations of rat coronary and cerebral arteries involve inward rectifier K(+) channels.* J Physiol, 1996. **492 (Pt 2)**: p. 419-30.
48. Eckman, D.M. and M.T. Nelson, *Potassium ions as vasodilators: role of inward rectifier potassium channels.* Circ Res, 2001. **88**(2): p. 132-3.
49. Horiuchi, T., et al., *Mechanism of extracellular K+-induced local and conducted responses in cerebral penetrating arterioles.* Stroke, 2002. **33**(11): p. 2692-9.
50. Dunn, K.M. and M.T. Nelson, *Potassium channels and neurovascular coupling.* Circ J, 2010. **74**(4): p. 608-16.
51. Girouard, H., et al., *Astrocytic endfoot Ca2+ and BK channels determine both arteriolar dilation and constriction.* Proc Natl Acad Sci U S A, 2010. **107**(8): p. 3811-6.
52. Attwell, D., et al., *Glial and neuronal control of brain blood flow.* Nature, 2010. **468**(7321): p. 232-43.
53. Hamilton, N.B., D. Attwell, and C.N. Hall, *Pericyte-mediated regulation of capillary diameter: a component of neurovascular coupling in health and disease.* Front Neuroenergetics, 2010. **2**.
54. Hirschi, K.K. and P.A. D'Amore, *Pericytes in the microvasculature.* Cardiovasc Res, 1996. **32**(4): p. 687-98.
55. Peppiatt, C.M., et al., *Bidirectional control of CNS capillary diameter by pericytes.* Nature, 2006. **443**(7112): p. 700-4.
56. Hall, C.N., et al., *Capillary pericytes regulate cerebral blood flow in health and disease.* Nature, 2014. **508**(7494): p. 55-60.
57. Shih, A.Y., et al., *Two-photon microscopy as a tool to study blood flow and neurovascular coupling in the rodent brain.* J Cereb Blood Flow Metab, 2012. **32**(7): p. 1277-309.
58. Prakash, N., et al., *Temporal profiles and 2-dimensional oxy-, deoxy-, and total-hemoglobin somatosensory maps in rat versus mouse cortex.* Neuroimage, 2007. **37 Suppl 1**: p. S27-36.
59. Adamczak, J.M., et al., *High field BOLD response to forepaw stimulation in the mouse.* Neuroimage, 2010. **51**(2): p. 704-12.
60. Drew, P.J., et al., *Chronic optical access through a polished and reinforced thinned skull.* Nat Methods, 2010. **7**(12): p. 981-4.
61. Kahn, I., et al., *Characterization of the functional MRI response temporal linearity via*

optical control of neocortical pyramidal neurons. J Neurosci, 2011. **31**(42): p. 15086-91.
62. Pisauro, M.A., et al., *Fast hemodynamic responses in the visual cortex of the awake mouse.* J Neurosci, 2013. **33**(46): p. 18343-51.
63. Grandjean, J., et al., *Optimization of anesthesia protocol for resting-state fMRI in mice based on differential effects of anesthetics on functional connectivity patterns.* Neuroimage, 2014. **102 Pt 2**: p. 838-47.
64. Schroeter, A., et al., *Specificity of stimulus-evoked fMRI responses in the mouse: the influence of systemic physiological changes associated with innocuous stimulation under four different anesthetics.* Neuroimage, 2014. **94**: p. 372-84.
65. Berwick, J., et al., *Hemodynamic response in the unanesthetized rat: intrinsic optical imaging and spectroscopy of the barrel cortex.* J Cereb Blood Flow Metab, 2002. **22**(6): p. 670-9.
66. Lahti, K.M., et al., *Comparison of evoked cortical activity in conscious and propofol-anesthetized rats using functional MRI.* Magn Reson Med, 1999. **41**(2): p. 412-6.
67. Peeters, R.R., et al., *Comparing BOLD fMRI signal changes in the awake and anesthetized rat during electrical forepaw stimulation.* Magn Reson Imaging, 2001. **19**(6): p. 821-6.
68. Chen, L.M., et al., *Fine-scale organization of SI (area 3b) in the squirrel monkey revealed with intrinsic optical imaging.* J Neurophysiol, 2001. **86**(6): p. 3011-29.
69. Martin, C., et al., *Investigating neural-hemodynamic coupling and the hemodynamic response function in the awake rat.* Neuroimage, 2006. **32**(1): p. 33-48.
70. Schlegel, F., A. Schroeter, and M. Rudin, *The hemodynamic response to somatosensory stimulation in mice depends on the anesthetic used: Implications on analysis of mouse fMRI data.* Neuroimage, 2015. **116**: p. 40-9.
71. Sokoloff, L., et al., *The [14C]deoxyglucose method for the measurement of local cerebral glucose utilization: theory, procedure, and normal values in the conscious and anesthetized albino rat.* J Neurochem, 1977. **28**(5): p. 897-916.
72. Kohro, S., et al., *Anesthetic effects on mitochondrial ATP-sensitive K channel.* Anesthesiology, 2001. **95**(6): p. 1435-340.
73. Rottenberg, H., *Uncoupling of oxidative phosphorylation in rat liver mitochondria by general anesthetics.* Proc Natl Acad Sci U S A, 1983. **80**(11): p. 3313-7.
74. Maekawa, T., et al., *Local cerebral blood flow and glucose utilization during isoflurane anesthesia in the rat.* Anesthesiology, 1986. **65**(2): p. 144-51.
75. Sicard, K., et al., *Regional cerebral blood flow and BOLD responses in conscious and anesthetized rats under basal and hypercapnic conditions: implications for functional MRI studies.* J Cereb Blood Flow Metab, 2003. **23**(4): p. 472-81.
76. Dudley, R.E., S.R. Nelson, and F. Samson, *Influence of chloralose on brain regional glucose utilization.* Brain Res, 1982. **233**(1): p. 173-80.
77. Ueki, M., G. Mies, and K.A. Hossmann, *Effect of alpha-chloralose, halothane, pentobarbital and nitrous oxide anesthesia on metabolic coupling in somatosensory cortex of rat.* Acta Anaesthesiol Scand, 1992. **36**(4): p. 318-22.
78. Hyder, F., D.L. Rothman, and R.G. Shulman, *Total neuroenergetics support localized brain activity: implications for the interpretation of fMRI.* Proc Natl Acad Sci U S A, 2002. **99**(16): p. 10771-6.
79. Crane, P.D., et al., *Dose dependent reduction of glucose utilization by pentobarbital in rat brain.* Stroke, 1978. **9**(1): p. 12-8.
80. Sakabe, T., et al., *Local cerebral glucose utilization during nitrous oxide and pentobarbital*

anesthesia in rats. Anesthesiology, 1985. **63**(3): p. 262-6.
81. Ingvar, M., A. Abdul-Rahman, and B.K. Siesjo, *Local cerebral glucose consumption in the artificially ventilated rat: influence of nitrous oxide analgesia and of phenobarbital anesthesia.* Acta Physiol Scand, 1980. **109**(2): p. 177-85.
82. Ndubuizu, O. and J.C. LaManna, *Brain tissue oxygen concentration measurements.* Antioxid Redox Signal, 2007. **9**(8): p. 1207-19.
83. Lyons, D.G., et al., *Mapping oxygen concentration in the awake mouse brain.* Elife, 2016. **5**.
84. Choi, D.H., et al., *Monitoring cerebral oxygenation and local field potential with a variation of isoflurane concentration in a rat model.* Biomed Opt Express, 2016. **7**(10): p. 4114-4124.
85. Bonvento, G., et al., *Is alpha-chloralose plus halothane induction a suitable anesthetic regimen for cerebrovascular research?* Brain Res, 1994. **665**(2): p. 213-21.
86. Franks, N.P., *General anaesthesia: from molecular targets to neuronal pathways of sleep and arousal.* Nat Rev Neurosci, 2008. **9**(5): p. 370-86.
87. Antunes, L.M., et al., *Comparison of electroencephalogram activity and auditory evoked responses during isoflurane and halothane anaesthesia in the rat.* Vet Anaesth Analg, 2003. **30**(1): p. 15-23.
88. Austin, V.C., et al., *Confounding effects of anesthesia on functional activation in rodent brain: a study of halothane and alpha-chloralose anesthesia.* Neuroimage, 2005. **24**(1): p. 92-100.
89. Ries, C.R. and E. Puil, *Mechanism of anesthesia revealed by shunting actions of isoflurane on thalamocortical neurons.* J Neurophysiol, 1999. **81**(4): p. 1795-801.
90. Alkire, M.T., A.G. Hudetz, and G. Tononi, *Consciousness and anesthesia.* Science, 2008. **322**(5903): p. 876-80.
91. Borg-Graham, L.J., C. Monier, and Y. Fregnac, *Visual input evokes transient and strong shunting inhibition in visual cortical neurons.* Nature, 1998. **393**(6683): p. 369-73.
92. Haider, B. and D.A. McCormick, *Rapid neocortical dynamics: cellular and network mechanisms.* Neuron, 2009. **62**(2): p. 171-89.
93. Haider, B., M. Hausser, and M. Carandini, *Inhibition dominates sensory responses in the awake cortex.* Nature, 2013. **493**(7430): p. 97-100.
94. Masamoto, K. and I. Kanno, *Anesthesia and the quantitative evaluation of neurovascular coupling.* J Cereb Blood Flow Metab, 2012. **32**(7): p. 1233-47.
95. Voss, L. and J. Sleigh, *Monitoring consciousness: the current status of EEG-based depth of anaesthesia monitors.* Best Pract Res Clin Anaesthesiol, 2007. **21**(3): p. 313-25.
96. Sellers, K.K., et al., *Anesthesia differentially modulates spontaneous network dynamics by cortical area and layer.* J Neurophysiol, 2013. **110**(12): p. 2739-51.
97. Thrane, A.S., et al., *General anesthesia selectively disrupts astrocyte calcium signaling in the awake mouse cortex.* Proc Natl Acad Sci U S A, 2012. **109**(46): p. 18974-9.
98. Raz, A., et al., *Preferential effect of isoflurane on top-down vs. bottom-up pathways in sensory cortex.* Front Syst Neurosci, 2014. **8**: p. 191.
99. Liang, Z., X. Liu, and N. Zhang, *Dynamic resting state functional connectivity in awake and anesthetized rodents.* Neuroimage, 2015. **104**: p. 89-99.
100. Nimmerjahn, A., E.A. Mukamel, and M.J. Schnitzer, *Motor behavior activates Bergmann glial networks.* Neuron, 2009. **62**(3): p. 400-12.
101. Flynn, N., et al., *Cerebral vascular responses to anesthetics.* Adv Exp Med Biol, 1991.

301: p. 237-46.
102. Flynn, N.M., et al., *Isoflurane produces endothelium-independent relaxation in canine middle cerebral arteries.* Anesthesiology, 1992. **76**(3): p. 461-7.
103. Lida, H., et al., *Isoflurane and sevoflurane induce vasodilation of cerebral vessels via ATP-sensitive K+ channel activation.* Anesthesiology, 1998. **89**(4): p. 954-60.
104. Buljubasic, N., et al., *Effects of isoflurane on K+ and Ca2+ conductance in isolated smooth muscle cells of canine cerebral arteries.* Anesth Analg, 1992. **75**(4): p. 590-6.
105. Akata, T., et al., *Mechanisms of direct inhibitory action of isoflurane on vascular smooth muscle of mesenteric resistance arteries.* Anesthesiology, 2003. **99**(3): p. 666-77.
106. Akata, T., *General anesthetics and vascular smooth muscle: direct actions of general anesthetics on cellular mechanisms regulating vascular tone.* Anesthesiology, 2007. **106**(2): p. 365-91.
107. Wheeler, D.M., et al., *Volatile anesthetic effects on sarcoplasmic reticulum Ca content and sarcolemmal Ca flux in isolated rat cardiac cell suspensions.* Anesthesiology, 1994. **80**(2): p. 372-82.
108. Yamamoto, M., et al., *Different effects of halothane, isoflurane and sevoflurane on sarcoplasmic reticulum of vascular smooth muscle in dog mesenteric artery.* Acta Anaesthesiol Scand, 1997. **41**(3): p. 376-80.
109. Muldoon, S.M., et al., *Attenuation of endothelium-mediated vasodilation by halothane.* Anesthesiology, 1988. **68**(1): p. 31-7.
110. Van Aken, H. and J. Van Hemelrijck, *Influence of anesthesia on cerebral blood flow and cerebral metabolism: an overview.* Agressologie, 1991. **32**(6-7): p. 303-6.
111. Weber, B., et al., *Optical imaging of the spatiotemporal dynamics of cerebral blood flow and oxidative metabolism in the rat barrel cortex.* Eur J Neurosci, 2004. **20**(10): p. 2664-70.
112. Hillman, E.M., *Optical brain imaging in vivo: techniques and applications from animal to man.* J Biomed Opt, 2007. **12**(5): p. 051402.
113. Liao, L.D., et al., *Neurovascular coupling: in vivo optical techniques for functional brain imaging.* Biomed Eng Online, 2013. **12**: p. 38.
114. Briers, J.D., *Laser Doppler, speckle and related techniques for blood perfusion mapping and imaging.* Physiol Meas, 2001. **22**(4): p. R35-66.
115. Briers, J.D., *Laser speckle contrast imaging for measuring blood flow.* Optica Applicata, 2007. **XXXVII**(1-2).
116. Grinvald, A., et al., *In-Vivo Optical Imaging of Cortical Architecture and Dynamics*, in *Modern Techniques in Neuroscience Research*, U. Windhorst and H. Johansson (Editors) Springer Verlag, Editor. 2001.
117. Devor, A., et al., *Two-Photon Laser Scanning Microscopy as a Tool to Study Cortical Vasodynamics Under Normal and Ischemic Conditions.* Imaging the Brain with Optical Methods, 2010: p. 245–261.
118. C.G., G. and G. J.A., *Super-resolution microscopy at a glance.* Journal of Cell Science, 2011. **124**: p. 1607-1611.
119. Oberg, P.A., T. Tenland, and G.E. Nilsson, *Laser-Doppler flowmetry--a non-invasive and continuous method for blood flow evaluation in microvascular studies.* Acta Med Scand Suppl, 1984. **687**: p. 17-24.
120. Dirnagl, U., et al., *Continuous measurement of cerebral cortical blood flow by laser-Doppler flowmetry in a rat stroke model.* J Cereb Blood Flow Metab, 1989. **9**(5): p. 589-

96.
121. Gu, W., W. Jiang, and P. Wester, *Real-time cortical cerebral blood flow follow-up in conscious, freely moving rats by laser Doppler flowmetry.* Methods, 2003. **30**(2): p. 172-7.
122. Hungerhuber, E., et al., *Simultaneous bilateral laser Doppler fluxmetry and electrophysiological recording during middle cerebral artery occlusion in rats.* J Neurosci Methods, 2006. **154**(1-2): p. 109-15.
123. Shepherd, A.P. and P.Å. Öberg, *Laser-Doppler blood flowmetry*. Developments in cardiovascular medicine DICM 107. 1990, Boston: Kluwer Academic Publishers. xv, 395 : ill. ; 25 cm.
124. Haberl, R.L., A. Villringer, and U. Dirnagl, *Applicability of laser-Doppler flowmetry for cerebral blood flow monitoring in neurological intensive care.* Acta Neurochir Suppl (Wien), 1993. **59**: p. 64-8.
125. Kirkpatrick, P.J., et al., *Continuous monitoring of cortical perfusion by laser Doppler flowmetry in ventilated patients with head injury.* J Neurol Neurosurg Psychiatry, 1994. **57**(11): p. 1382-8.
126. Donnelly, J., et al., *Regulation of the cerebral circulation: bedside assessment and clinical implications.* Crit Care, 2016. **20**(1): p. 129.
127. Haberl, R.L., M.L. Heizer, and E.F. Ellis, *Laser-Doppler assessment of brain microcirculation: effect of local alterations.* Am J Physiol, 1989. **256**(4 Pt 2): p. H1255-60.
128. Uranishi, R., et al., *Evaluation of absolute cerebral blood flow by laser-Doppler scanning-- comparison with hydrogen clearance.* J Vasc Res, 1999. **36**(2): p. 100-5.
129. Matsuura, T. and I. Kanno, *Changes in red blood cell behavior during cerebral blood flow increase in the rat somatosensory cortex: a study of laser-Doppler flowmetry.* Jpn J Physiol, 2001. **51**(6): p. 703-8.
130. Winfree, C.J., et al., *Laser Doppler flowmetry in non-human primate stroke studies: model refinement for pre-clinical development of cerebroprotective strategies.* Acta Neurochir (Wien), 2003. **145**(12): p. 1105-10; discussion 1110.
131. He, J., et al., *Simultaneous laser Doppler flowmetry and arterial spin labeling MRI for measurement of functional perfusion changes in the cortex.* Neuroimage, 2007. **34**(4): p. 1391-404.
132. Takuwa, H., et al., *Hemodynamic changes during somatosensory stimulation in awake and isoflurane-anesthetized mice measured by laser-Doppler flowmetry.* Brain Res, 2012. **1472**: p. 107-12.
133. Takuwa, H., et al., *Hemodynamic changes during neural deactivation in awake mice: a measurement by laser-Doppler flowmetry in crossed cerebellar diaschisis.* Brain Res, 2013. **1537**: p. 350-5.
134. Satomura, S., S. Matsubara, and M. Yoshioka, *A new method of mechanical vibration measurement and its application.* Memoirs Inst Sci Indust Res Osaka Univ, 1956. **13**: p. 123-133.
135. Riva, C., B. Ross, and G.B. Benedek, *Laser Doppler measurements of blood flow in capillary tubes and retinal arteries.* Invest Ophthalmol, 1972. **11**(11): p. 936-44.
136. Holloway, G.A., Jr. and D.W. Watkins, *Laser Doppler measurement of cutaneous blood flow.* J Invest Dermatol, 1977. **69**(3): p. 306-9.
137. Bonner, R. and R. Nossal, *Model for laser Doppler measurements of blood flow in tissue.*

Appl Opt, 1981. **20**(12): p. 2097-107.
138. Niwa, K., et al., *Abeta 1-40-related reduction in functional hyperemia in mouse neocortex during somatosensory activation.* Proc Natl Acad Sci U S A, 2000. **97**(17): p. 9735-40.
139. Ayata, C., et al., *Laser speckle flowmetry for the study of cerebrovascular physiology in normal and ischemic mouse cortex.* J Cereb Blood Flow Metab, 2004. **24**(7): p. 744-55.
140. Takuwa, H., et al., *Reproducibility and variance of a stimulation-induced hemodynamic response in barrel cortex of awake behaving mice.* Brain Res, 2011. **1369**: p. 103-11.
141. Haberl, R.L., et al., *Laser-Doppler assessment of brain microcirculation: effect of systemic alterations.* Am J Physiol, 1989. **256**(4 Pt 2): p. H1247-54.
142. Mayhew, J., et al., *Spectroscopic investigation of reflectance changes in the barrel cortex following whisker stimulation.* Adv Exp Med Biol, 1998. **454**: p. 139-48.
143. Boyle, N.H., et al., *Scanning laser Doppler is a useful technique to assess foot cutaneous perfusion during femoral artery cannulation.* Crit Care, 1999. **3**(4): p. 95-100.
144. Nielsen, A.N., M. Fabricius, and M. Lauritzen, *Scanning laser-Doppler flowmetry of rat cerebral circulation during cortical spreading depression.* J Vasc Res, 2000. **37**(6): p. 513-22.
145. Lauritzen, M. and M. Fabricius, *Real time laser-Doppler perfusion imaging of cortical spreading depression in rat neocortex.* Neuroreport, 1995. **6**(9): p. 1271-3.
146. Ances, B.M., J.H. Greenberg, and J.A. Detre, *Laser doppler imaging of activation-flow coupling in the rat somatosensory cortex.* Neuroimage, 1999. **10**(6): p. 716-23.
147. Nossal, R., R.F. Bonner, and G.H. Weiss, *Influence of path length on remote optical sensing of properties of biological tissue.* Appl Opt, 1989. **28**(12): p. 2238-44.
148. Larsson, M., W. Steenbergen, and T. Stromberg, *Influence of optical properties and fiber separation on laser doppler flowmetry.* J Biomed Opt, 2002. **7**(2): p. 236-43.
149. Nilsson, H., et al., *Photon pathlength determination based on spatially resolved diffuse reflectance.* J Biomed Opt, 2002. **7**(3): p. 478-85.
150. Kuroiwa, T., P. Bonnekoh, and K.A. Hossmann, *Laser doppler flowmetry in CA1 sector of hippocampus and cortex after transient forebrain ischemia in gerbils.* Stroke, 1992. **23**(9): p. 1349-54.
151. Fabricius, M., et al., *Laminar analysis of cerebral blood flow in cortex of rats by laser-Doppler flowmetry: a pilot study.* J Cereb Blood Flow Metab, 1997. **17**(12): p. 1326-36.
152. Barfod, C., et al., *Laser-Doppler measurements of concentration and velocity of moving blood cells in rat cerebral circulation.* Acta Physiol Scand, 1997. **160**(2): p. 123-32.
153. Frerichs, K.U. and G.Z. Feuerstein, *Laser-Doppler flowmetry. A review of its application for measuring cerebral and spinal cord blood flow.* Mol Chem Neuropathol, 1990. **12**(1): p. 55-70.
154. de Mul, F.F., et al., *Mini laser-Doppler (blood) flow monitor with diode laser source and detection integrated in the probe.* Appl Opt, 1984. **23**(17): p. 2970.
155. Kimura, Y., et al., *Integrated laser Doppler blood flowmeter designed to enable wafer-level packaging.* IEEE Trans Biomed Eng, 2010. **57**(8): p. 2026-33.
156. Serov, A.N., et al., *Integrated optoelectronic probe including a vertical cavity surface emitting laser for laser Doppler perfusion monitoring.* IEEE Trans Biomed Eng, 2006. **53**(10): p. 2067-74.
157. Sato, A., S. Uchida, and Y. Yamauchi, *A new method for continuous measurement of regional cerebral blood flow using laser Doppler flowmetry in a conscious rat.* Neurosci Lett, 1994. **175**(1-2): p. 149-52.

158. Tajima, Y., et al., *Reproducibility of measuring cerebral blood flow by laser-Doppler flowmetry in mice.* Front Biosci (Elite Ed), 2014. **6**: p. 62-8.
159. Fercher, A.F. and J.D. Briers, *Flow visualization by means of single-exposure speckle photography.* Opt Commun, 1981. **37**: p. 327-330.
160. Dunn, A.K., *Laser speckle contrast imaging of cerebral blood flow.* Ann Biomed Eng, 2012. **40**(2): p. 367-77.
161. Strong, A.J., et al., *Evaluation of laser speckle flowmetry for imaging cortical perfusion in experimental stroke studies: quantitation of perfusion and detection of peri-infarct depolarisations.* J Cereb Blood Flow Metab, 2006. **26**(5): p. 645-53.
162. Murari, K., et al., *Contrast-enhanced imaging of cerebral vasculature with laser speckle.* Appl Opt, 2007. **46**(22): p. 5340-6.
163. Boas, D.A. and A.K. Dunn, *Laser speckle contrast imaging in biomedical optics.* J Biomed Opt, 2010. **15**(1): p. 011109.
164. Murari, K., et al., *Design and characterization of a miniaturized epi-illuminated microscope.* Conf Proc IEEE Eng Med Biol Soc, 2009. **2009**: p. 5369-72.
165. Miao, P., et al., *Laser speckle contrast imaging of cerebral blood flow in freely moving animals.* J Biomed Opt, 2011. **16**(9): p. 090502.
166. Miao, P., et al., *Random process estimator for laser speckle imaging of cerebral blood flow.* Opt Express, 2010. **18**(1): p. 218-36.
167. Parthasarathy, A.B., et al., *Laser speckle contrast imaging of cerebral blood flow in humans during neurosurgery: a pilot clinical study.* J Biomed Opt, 2010. **15**(6): p. 066030.
168. Frostig, R.D., et al., *Cortical functional architecture and local coupling between neuronal activity and the microcirculation revealed by in vivo high-resolution optical imaging of intrinsic signals.* Proc Natl Acad Sci U S A, 1990. **87**(16): p. 6082-6.
169. Malonek, D., et al., *Vascular imprints of neuronal activity: relationships between the dynamics of cortical blood flow, oxygenation, and volume changes following sensory stimulation.* Proc Natl Acad Sci U S A, 1997. **94**(26): p. 14826-31.
170. Mayhew, J., et al., *Spectroscopic analysis of changes in remitted illumination: the response to increased neural activity in brain.* Neuroimage, 1999. **10**(3 Pt 1): p. 304-26.
171. Hess, A., et al., *New insights into the hemodynamic blood oxygenation level-dependent response through combination of functional magnetic resonance imaging and optical recording in gerbil barrel cortex.* J Neurosci, 2000. **20**(9): p. 3328-38.
172. Blood, A.J., N. Pouratian, and A.W. Toga, *Temporally staggered forelimb stimulation modulates barrel cortex optical intrinsic signal responses to whisker stimulation.* J Neurophysiol, 2002. **88**(1): p. 422-37.
173. Devor, A., et al., *Coupling of total hemoglobin concentration, oxygenation, and neural activity in rat somatosensory cortex.* Neuron, 2003. **39**(2): p. 353-9.
174. Martindale, J., et al., *The hemodynamic impulse response to a single neural event.* J Cereb Blood Flow Metab, 2003. **23**(5): p. 546-55.
175. Sheth, S.A., et al., *Linear and nonlinear relationships between neuronal activity, oxygen metabolism, and hemodynamic responses.* Neuron, 2004. **42**(2): p. 347-55.
176. Berwick, J., et al., *Neurovascular coupling investigated with two-dimensional optical imaging spectroscopy in rat whisker barrel cortex.* Eur J Neurosci, 2005. **22**(7): p. 1655-66.
177. Vanzetta, I., R. Hildesheim, and A. Grinvald, *Compartment-resolved imaging of activity-dependent dynamics of cortical blood volume and oximetry.* J Neurosci, 2005. **25**(9): p.

2233-44.
178. Berwick, J., et al., *Fine detail of neurovascular coupling revealed by spatiotemporal analysis of the hemodynamic response to single whisker stimulation in rat barrel cortex.* J Neurophysiol, 2008. **99**(2): p. 787-98.
179. Boorman, L., et al., *Negative blood oxygen level dependence in the rat: a model for investigating the role of suppression in neurovascular coupling.* J Neurosci, 2010. **30**(12): p. 4285-94.
180. Martin, C., et al., *Complex spatiotemporal haemodynamic response following sensory stimulation in the awake rat.* Neuroimage, 2013. **66**: p. 1-8.
181. Ma, Z., et al., *Inverted optical intrinsic response accompanied by decreased cerebral blood flow are related to both neuronal inhibition and excitation.* Sci Rep, 2016. **6**: p. 21627.
182. Frostig, R.D., Z. Frostig, and R.M. Harper, *Recurring discharge patterns in multiple spike trains. I. Detection.* Biol Cybern, 1990. **62**(6): p. 487-93.
183. Bonhoeffer, T., *Optical imaging of intrinsic signals as a tool to visualize the functional architecture of adult and developing visual cortex.* Arzneimittelforschung, 1995. **45**(3A): p. 351-6.
184. Mayhew, J., et al., *Spectroscopic analysis of neural activity in brain: increased oxygen consumption following activation of barrel cortex.* Neuroimage, 2000. **12**(6): p. 664-75.
185. Ratzlaff, E.H. and A. Grinvald, *A tandem-lens epifluorescence macroscope: hundred-fold brightness advantage for wide-field imaging.* J Neurosci Methods, 1991. **36**(2-3): p. 127-37.
186. Elwell, C.E., et al., *Measurement of adult cerebral haemodynamics using near infrared spectroscopy.* Acta Neurochir Suppl (Wien), 1993. **59**: p. 74-80.
187. Boas, D.A., et al., *The accuracy of near infrared spectroscopy and imaging during focal changes in cerebral hemodynamics.* Neuroimage, 2001. **13**(1): p. 76-90.
188. Vnek, N., et al., *Optical imaging of functional domains in the cortex of the awake and behaving monkey.* Proc Natl Acad Sci U S A, 1999. **96**(7): p. 4057-60.
189. Rector, D.M., et al., *A miniature CCD video camera for high-sensitivity light measurements in freely behaving animals.* J Neurosci Methods, 1997. **78**(1-2): p. 85-91.
190. Martin, C., et al., *Optical imaging spectroscopy in the unanaesthetised rat.* J Neurosci Methods, 2002. **120**(1): p. 25-34.
191. Sharp, P.S., et al., *Comparison of stimulus-evoked cerebral hemodynamics in the awake mouse and under a novel anesthetic regime.* Sci Rep, 2015. **5**: p. 12621.
192. Dunn, A.K., et al., *Simultaneous imaging of total cerebral hemoglobin concentration, oxygenation, and blood flow during functional activation.* Opt Lett, 2003. **28**(1): p. 28-30.
193. Sheth, S.A., et al., *Spatiotemporal evolution of functional hemodynamic changes and their relationship to neuronal activity.* J Cereb Blood Flow Metab, 2005. **25**(7): p. 830-41.
194. Haglund, M.M. and D.W. Hochman, *Optical imaging of epileptiform activity in human neocortex.* Epilepsia, 2004. **45 Suppl 4**: p. 43-7.
195. Pouratian, N., et al., *Applications and limitations of perfusion-dependent functional brain mapping for neurosurgical guidance.* Neurosurg Focus, 2003. **15**(1): p. E2.
196. Pouratian, N., et al., *Shedding light on brain mapping: advances in human optical imaging.* Trends Neurosci, 2003. **26**(5): p. 277-82.
197. Grinvald, A., et al., *In-vivo Optical imaging of cortical architecture and dynamics.* Modern Techniques in Neuroscience Research, 1999: p. 893-969.
198. Harrison, R.V., et al., *Optical imaging of intrinsic signals in chinchilla auditory cortex.*

Audiol Neurootol, 1998. **3**(2-3): p. 214-23.
199. Jung, J.C., et al., *In vivo mammalian brain imaging using one- and two-photon fluorescence microendoscopy.* J Neurophysiol, 2004. **92**(5): p. 3121-33.
200. Levene, M.J., et al., *In vivo multiphoton microscopy of deep brain tissue.* J Neurophysiol, 2004. **91**(4): p. 1908-12.
201. Barretto, R.P., B. Messerschmidt, and M.J. Schnitzer, *In vivo fluorescence imaging with high-resolution microlenses.* Nat Methods, 2009. **6**(7): p. 511-2.
202. Simard, M., et al., *Signaling at the gliovascular interface.* J Neurosci, 2003. **23**(27): p. 9254-62.
203. Zonta, M., et al., *Neuron-to-astrocyte signaling is central to the dynamic control of brain microcirculation.* Nat Neurosci, 2003. **6**(1): p. 43-50.
204. Cauli, B., et al., *Cortical GABA interneurons in neurovascular coupling: relays for subcortical vasoactive pathways.* J Neurosci, 2004. **24**(41): p. 8940-9.
205. Mulligan, S.J. and B.A. MacVicar, *Calcium transients in astrocyte endfeet cause cerebrovascular constrictions.* Nature, 2004. **431**(7005): p. 195-9.
206. Rancillac, A., et al., *Glutamatergic Control of Microvascular Tone by Distinct GABA Neurons in the Cerebellum.* J Neurosci, 2006. **26**(26): p. 6997-7006.
207. Faraci, F.M. and K.R. Breese, *Nitric oxide mediates vasodilatation in response to activation of N-methyl-D-aspartate receptors in brain.* Circ Res, 1993. **72**(2): p. 476-80.
208. Kleinfeld, D., et al., *Fluctuations and stimulus-induced changes in blood flow observed in individual capillaries in layers 2 through 4 of rat neocortex.* Proc Natl Acad Sci U S A, 1998. **95**(26): p. 15741-6.
209. Chaigneau, E., et al., *Two-photon imaging of capillary blood flow in olfactory bulb glomeruli.* Proc Natl Acad Sci U S A, 2003. **100**(22): p. 13081-6.
210. Takano, T., et al., *Astrocyte-mediated control of cerebral blood flow.* Nat Neurosci, 2006. **9**(2): p. 260-7.
211. Chaigneau, E., et al., *The relationship between blood flow and neuronal activity in the rodent olfactory bulb.* J Neurosci, 2007. **27**(24): p. 6452-60.
212. Devor, A., et al., *Suppressed neuronal activity and concurrent arteriolar vasoconstriction may explain negative blood oxygenation level-dependent signal.* J Neurosci, 2007. **27**(16): p. 4452-9.
213. Zhang, S. and T.H. Murphy, *Imaging the impact of cortical microcirculation on synaptic structure and sensory-evoked hemodynamic responses in vivo.* PLoS Biol, 2007. **5**(5): p. e119.
214. Denk, W., J.H. Strickler, and W.W. Webb, *Two-photon laser scanning fluorescence microscopy.* Science, 1990. **248**(4951): p. 73-6.
215. Helmchen, F. and W. Denk, *Deep tissue two-photon microscopy.* Nat Methods, 2005. **2**(12): p. 932-40.
216. Svoboda, K. and R. Yasuda, *Principles of two-photon excitation microscopy and its applications to neuroscience.* Neuron, 2006. **50**(6): p. 823-39.
217. Frostig, R.D., *In vivo optical imaging of brain function*. Frontiers in neuroscience. 2009, Boca Raton, Fla. ; London: CRC Press. xv, 472 , 16 of plates : ill. (some col.) ; 25 cm.
218. Smith, L.E., et al., *Oxygen-induced retinopathy in the mouse.* Invest Ophthalmol Vis Sci, 1994. **35**(1): p. 101-11.
219. Chuquet, J., L. Hollender, and E.A. Nimchinsky, *High-resolution in vivo imaging of the neurovascular unit during spreading depression.* J Neurosci, 2007. **27**(15): p. 4036-44.

220. Helmchen, F., et al., *A miniature head-mounted two-photon microscope. high-resolution brain imaging in freely moving animals.* Neuron, 2001. **31**(6): p. 903-12.
221. Drew, P.J., A.Y. Shih, and D. Kleinfeld, *Fluctuating and sensory-induced vasodynamics in rodent cortex extend arteriole capacity.* Proc Natl Acad Sci U S A, 2011. **108**(20): p. 8473-8.
222. Song, A., et al., *Volumetric two-photon imaging of neurons using stereoscopy (vTwINS).* Nat Methods, 2017. **14**(4): p. 420-426.
223. Obrenovitch, T.P., S. Chen, and E. Farkas, *Simultaneous, live imaging of cortical spreading depression and associated cerebral blood flow changes, by combining voltage-sensitive dye and laser speckle contrast methods.* Neuroimage, 2009. **45**(1): p. 68-74.
224. Yakovlev, V.V., et al., *Stimulated Raman photoacoustic imaging.* Proc Natl Acad Sci U S A, 2010. **107**(47): p. 20335-9.
225. Liu, T., et al., *Combined photoacoustic microscopy and optical coherence tomography can measure metabolic rate of oxygen.* Biomed Opt Express, 2011. **2**(5): p. 1359-65.
226. Wang, Y., et al., *In vivo integrated photoacoustic and confocal microscopy of hemoglobin oxygen saturation and oxygen partial pressure.* Opt Lett, 2011. **36**(7): p. 1029-31.
227. Yao, J., et al., *Noninvasive photoacoustic computed tomography of mouse brain metabolism in vivo.* Neuroimage, 2013. **64**: p. 257-66.
228. Ma, H., M. Zhao, and T.H. Schwartz, *Dynamic neurovascular coupling and uncoupling during ictal onset, propagation, and termination revealed by simultaneous in vivo optical imaging of neural activity and local blood volume.* Cereb Cortex, 2013. **23**(4): p. 885-99.
229. Klohs, J., et al., *Imaging of cerebrovascular pathology in animal models of Alzheimer's disease.* Front Aging Neurosci, 2014. **6**: p. 32.
230. Ringuette, D., et al., *Multi-modal in vivo imaging of brain blood oxygenation, blood flow and neural calcium dynamics during acute seizures.* Proc. SPIE, 2016. **9690**.
231. Takuwa, H., et al., *Development of a simultaneous optical/PET imaging system for awake mice.* Phys Med Biol, 2016. **61**(17): p. 6430-40.
232. Arenkiel, B.R., et al., *In vivo light-induced activation of neural circuitry in transgenic mice expressing channelrhodopsin-2.* Neuron, 2007. **54**(2): p. 205-18.
233. Miesenbock, G., *Optogenetic control of cells and circuits.* Annu Rev Cell Dev Biol, 2011. **27**: p. 731-58.
234. Devor, A., et al., *Frontiers in optical imaging of cerebral blood flow and metabolism.* J Cereb Blood Flow Metab, 2012. **32**(7): p. 1259-76.
235. Rungta, R.L., et al., *Light controls cerebral blood flow in naive animals.* Nat Commun, 2017. **8**: p. 14191.
236. Kety, S.S., *Circulation and metabolism of the human brain in health and disease.* Am J Med, 1950. **8**(2): p. 205-17.
237. Ingvar, D.H., et al., *Activation patterns induced in the dominant hemisphere by skin stimulation*, in *Sensory Functions of the Skin in Primates*, Z. Y., Editor. 1976, Pergamon Press: Oxford. p. 542-549.
238. Carlsson, C., M. Hagerdal, and B.K. Siesjo, *Increase in cerebral oxygen uptake and blood flow in immobilization stress.* Acta Physiol Scand, 1975. **95**(2): p. 206-8.
239. Carlsson, C., et al., *A catecholamine-mediated increase in cerebral oxygen uptake during immobilisation stress in rats.* Brain Res, 1977. **119**(1): p. 223-31.
240. Hemmingsen, R., et al., *Cerebral blood flow and oxygen consumption during ethanol withdrawal in the rat.* Brain Res, 1979. **173**(2): p. 259-69.

241. Newman, L.M., et al., *Regional blood flow and cerebral metabolic changes during alcohol withdrawal and following midazolam therapy.* Anesthesiology, 1985. **63**(4): p. 395-400.
242. Chen, R.Y., et al., *Regional cerebral blood flow and oxygen consumption of the canine brain during hemorrhagic hypotension.* Stroke, 1984. **15**(2): p. 343-50.
243. Berntman, L., N. Dahlgren, and B.K. Siesjo, *Cerebral blood flow and oxygen consumption in the rat brain during extreme hypercarbia.* Anesthesiology, 1979. **50**(4): p. 299-305.
244. Traystman, R.J., R.S. Fitzgerald, and S.C. Loscutoff, *Cerebral circulatory responses to arterial hypoxia in normal and chemodenervated dogs.* Circ Res, 1978. **42**(5): p. 649-57.
245. Bryan, R.M., Jr. and R.A. Lehman, *Cerebral glucose utilization after aversive conditioning and during conditioned fear in the rat.* Brain Res, 1988. **444**(1): p. 17-24.
246. LeDoux, J.E., et al., *Local cerebral blood flow increases during auditory and emotional processing in the conscious rat.* Science, 1983. **221**(4610): p. 576-8.
247. Ohata, M., et al., *Effects of immobilization stress on regional cerebral blood flow in the conscious rat.* J Cereb Blood Flow Metab, 1981. **1**(2): p. 187-94.
248. Ohata, M., et al., *Effects of immobilization stress on cerebral blood flow and cerebrovascular permeability in spontaneously hypertensive rats.* J Cereb Blood Flow Metab, 1982. **2**(3): p. 373-9.
249. Schasfoort, E.M., L.A. De Bruin, and J. Korf, *Mild stress stimulates rat hippocampal glucose utilization transiently via NMDA receptors, as assessed by lactography.* Brain Res, 1988. **475**(1): p. 58-63.
250. Rahman, M.M., et al., *Chronic immobilization stress occludes in vivo cortical activation in an animal model of panic induced by carbon dioxide inhalation.* Front Behav Neurosci, 2014. **8**: p. 311.
251. Lee, S., et al., *Chronic Stress Decreases Cerebrovascular Responses During Rat Hindlimb Electrical Stimulation.* Front Neurosci, 2015. **9**: p. 462.
252. Fuchs, E., G. Flugge, and B. Czeh, *Remodeling of neuronal networks by stress.* Front Biosci, 2006. **11**: p. 2746-58.
253. Pawlak, R., et al., *Tissue plasminogen activator in the amygdala is critical for stress-induced anxiety-like behavior.* Nat Neurosci, 2003. **6**(2): p. 168-74.
254. Makino, S., et al., *Regulation of corticotropin-releasing hormone receptor messenger ribonucleic acid in the rat brain and pituitary by glucocorticoids and stress.* Endocrinology, 1995. **136**(10): p. 4517-25.
255. Cordero, M.I., et al., *Chronic restraint stress down-regulates amygdaloid expression of polysialylated neural cell adhesion molecule.* Neuroscience, 2005. **133**(4): p. 903-10.
256. Rajkowska, G. and J.J. Miguel-Hidalgo, *Gliogenesis and glial pathology in depression.* CNS Neurol Disord Drug Targets, 2007. **6**(3): p. 219-33.
257. Czeh, B. and P.J. Lucassen, *What causes the hippocampal volume decrease in depression? Are neurogenesis, glial changes and apoptosis implicated?* Eur Arch Psychiatry Clin Neurosci, 2007. **257**(5): p. 250-60.
258. Sabolek, M., et al., *Dexamethasone blocks astroglial differentiation from neural precursor cells.* Neuroreport, 2006. **17**(16): p. 1719-23.
259. Morimoto, M., et al., *Distribution of glucocorticoid receptor immunoreactivity and mRNA in the rat brain: an immunohistochemical and in situ hybridization study.* Neurosci Res, 1996. **26**(3): p. 235-69.
260. Virgin, C.E., Jr., et al., *Glucocorticoids inhibit glucose transport and glutamate uptake in hippocampal astrocytes: implications for glucocorticoid neurotoxicity.* J Neurochem,

1991. **57**(4): p. 1422-8.
261. Simard, M., et al., *Glucocorticoids-potent modulators of astrocytic calcium signaling.* Glia, 1999. **28**(1): p. 1-12.
262. O'Donnell, J., et al., *Norepinephrine: a neuromodulator that boosts the function of multiple cell types to optimize CNS performance.* Neurochem Res, 2012. **37**(11): p. 2496-512.
263. Hertz, L., L. Peng, and G.A. Dienel, *Energy metabolism in astrocytes: high rate of oxidative metabolism and spatiotemporal dependence on glycolysis/glycogenolysis.* J Cereb Blood Flow Metab, 2007. **27**(2): p. 219-49.
264. Chatterjee, S. and S.K. Sikdar, *Corticosterone treatment results in enhanced release of peptidergic vesicles in astrocytes via cytoskeletal rearrangements.* Glia, 2013. **61**(12): p. 2050-62.
265. Nair, A. and R.H. Bonneau, *Stress-induced elevation of glucocorticoids increases microglia proliferation through NMDA receptor activation.* J Neuroimmunol, 2006. **171**(1-2): p. 72-85.
266. Tynan, R.J., et al., *Chronic stress alters the density and morphology of microglia in a subset of stress-responsive brain regions.* Brain Behav Immun, 2010. **24**(7): p. 1058-68.
267. You, Z., et al., *Pro- and anti-inflammatory cytokines expression in rat's brain and spleen exposed to chronic mild stress: involvement in depression.* Behav Brain Res, 2011. **225**(1): p. 135-41.
268. Goodwin, J.E., J. Zhang, and D.S. Geller, *A critical role for vascular smooth muscle in acute glucocorticoid-induced hypertension.* J Am Soc Nephrol, 2008. **19**(7): p. 1291-9.
269. Goodwin, J.E., et al., *Endothelial glucocorticoid receptor is required for protection against sepsis.* Proc Natl Acad Sci U S A, 2013. **110**(1): p. 306-11.
270. Dombeck, D.A., et al., *Imaging large-scale neural activity with cellular resolution in awake, mobile mice.* Neuron, 2007. **56**(1): p. 43-57.
271. Bryant, J.L., S. Roy, and D.H. Heck, *A technique for stereotaxic recordings of neuronal activity in awake, head-restrained mice.* J Neurosci Methods, 2009. **178**(1): p. 75-9.
272. Haiss, F., S. Butovas, and C. Schwarz, *A miniaturized chronic microelectrode drive for awake behaving head restrained mice and rats.* J Neurosci Methods, 2010. **187**(1): p. 67-72.
273. Muniak, M.A., et al., *Preparation of an awake mouse for recording neural responses and injecting tracers.* J Vis Exp, 2012(64).
274. Kislin, M., et al., *Flat-floored air-lifted platform: a new method for combining behavior with microscopy or electrophysiology on awake freely moving rodents.* J Vis Exp, 2014(88): p. e51869.
275. Mandelblat-Cerf, Y., et al., *Arcuate hypothalamic AgRP and putative POMC neurons show opposite changes in spiking across multiple timescales.* Elife, 2015. **4**(07122).
276. Tran, C.H. and G.R. Gordon, *Acute two-photon imaging of the neurovascular unit in the cortex of active mice.* Front Cell Neurosci, 2015. **9**: p. 11.
277. Holtmaat, A., et al., *Long-term, high-resolution imaging in the mouse neocortex through a chronic cranial window.* Nat Protoc, 2009. **4**(8): p. 1128-44.
278. Shih, A.Y., et al., *A polished and reinforced thinned-skull window for long-term imaging of the mouse brain.* J Vis Exp, 2012(61).
279. Gong, S., et al., *Dynamics and correlation of serum cortisol and corticosterone under different physiological or stressful conditions in mice.* PLoS One, 2015. **10**(2): p. e0117503.

280. Brammer, A., C.D. West, and S.L. Allen, *A comparison of propofol with other injectable anaesthetics in a rat model for measuring cardiovascular parameters.* Lab Anim, 1993. **27**(3): p. 250-7.
281. Fox, P.T. and M.E. Raichle, *Focal physiological uncoupling of cerebral blood flow and oxidative metabolism during somatosensory stimulation in human subjects.* Proc Natl Acad Sci U S A, 1986. **83**(4): p. 1140-4.
282. Andermann, M.L., A.M. Kerlin, and R.C. Reid, *Chronic cellular imaging of mouse visual cortex during operant behavior and passive viewing.* Front Cell Neurosci, 2010. **4**: p. 3.
283. Takuwa, H., et al., *Contribution of nitric oxide to cerebral blood flow regulation under hypoxia in rats.* J Physiol Sci, 2010. **60**(6): p. 399-406.
284. Chen, J.L., et al., *Imaging neuronal populations in behaving rodents: paradigms for studying neural circuits underlying behavior in the mammalian cortex.* J Neurosci, 2013. **33**(45): p. 17631-40.
285. Vaiceliunaite, A., et al., *Spatial integration in mouse primary visual cortex.* J Neurophysiol, 2013. **110**(4): p. 964-72.
286. Cazakoff, B.N., et al., *Broadly tuned and respiration-independent inhibition in the olfactory bulb of awake mice.* Nat Neurosci, 2014. **17**(4): p. 569-76.
287. Lecoq, J., et al., *Visualizing mammalian brain area interactions by dual-axis two-photon calcium imaging.* Nat Neurosci, 2014. **17**(12): p. 1825-9.
288. Mandelblat-Cerf, Y., et al., *Arcuate hypothalamic AgRP and putative POMC neurons show opposite changes in spiking across multiple timescales.* Elife, 2015. **4**.
289. Nishino, A., et al., *Vasodilation Mechanism of Cerebral Microvessels Induced by Neural Activation under High Baseline Cerebral Blood Flow Level Results from Hypercapnia in Awake Mice.* Microcirculation, 2015. **22**(8): p. 744-52.
290. Sekiguchi, K.J., et al., *Imaging large-scale cellular activity in spinal cord of freely behaving mice.* Nat Commun, 2016. **7**: p. 11450.
291. Murphy, T.H., et al., *High-throughput automated home-cage mesoscopic functional imaging of mouse cortex.* Nat Commun, 2016. **7**: p. 11611.
292. Schwarz, C., et al., *The head-fixed behaving rat--procedures and pitfalls.* Somatosens Mot Res, 2010. **27**(4): p. 131-48.
293. Dombeck, D.A., M.S. Graziano, and D.W. Tank, *Functional clustering of neurons in motor cortex determined by cellular resolution imaging in awake behaving mice.* J Neurosci, 2009. **29**(44): p. 13751-60.
294. Sofroniew, N.J., et al., *Natural whisker-guided behavior by head-fixed mice in tactile virtual reality.* J Neurosci, 2014. **34**(29): p. 9537-50.
295. Kolber, B.J., L. Wieczorek, and L.J. Muglia, *Hypothalamic-pituitary-adrenal axis dysregulation and behavioral analysis of mouse mutants with altered glucocorticoid or mineralocorticoid receptor function.* Stress, 2008. **11**(5): p. 321-38.
296. Smith, S.M. and W.W. Vale, *The role of the hypothalamic-pituitary-adrenal axis in neuroendocrine responses to stress.* Dialogues Clin Neurosci, 2006. **8**(4): p. 383-95.
297. Scaccianoce, S., K. Lombardo, and L. Angelucci, *Nerve growth factor brain concentration and stress: changes depend on type of stressor and age.* Int J Dev Neurosci, 2000. **18**(4-5): p. 469-79.
298. Longordo, F., et al., *Do mice habituate to "gentle handling?" A comparison of resting behavior, corticosterone levels and synaptic function in handled and undisturbed C57BL/6J mice.* Sleep, 2011. **34**(5): p. 679-81.

299. Baba, J.S., et al., *Molecular imaging of conscious, unrestrained mice with AwakeSPECT.* J Nucl Med, 2013. **54**(6): p. 969-76.
300. Mizuma, H., et al., *Establishment of in vivo brain imaging method in conscious mice.* J Nucl Med, 2010. **51**(7): p. 1068-75.
301. King, J.A., et al., *Procedure for minimizing stress for fMRI studies in conscious rats.* J Neurosci Methods, 2005. **148**(2): p. 154-60.
302. Kaisti, K.K., et al., *Effects of surgical levels of propofol and sevoflurane anesthesia on cerebral blood flow in healthy subjects studied with positron emission tomography.* Anesthesiology, 2002. **96**(6): p. 1358-70.
303. Schulz, D., et al., *Simultaneous assessment of rodent behavior and neurochemistry using a miniature positron emission tomograph.* Nat Methods, 2011. **8**(4): p. 347-52.
304. Seibenhener, M.L. and M.C. Wooten, *Use of the Open Field Maze to measure locomotor and anxiety-like behavior in mice.* J Vis Exp, 2015(96): p. e52434.
305. Wilson, G.T. and G.C. Davison, *Processes of fear reduction in systematic desensitization: animal studies.* Psychol Bull, 1971. **76**(1): p. 1-14.